DIELECTRIC ELASTOMERS AS POTENTIAL ACTUATING ELEMENTS OF RECONFIGURABLE ANTENNAS

by

Kambiz Daheshpour

B.A.Sc., Electrical Engineering, University of Ottawa, 2007

THESIS SUBMITTED IN PARTIAL FULFILLMENT OF
THE REQUIREMENTS FOR THE DEGREE OF

MASTER OF APPLIED SCIENCE

In the
School of Engineering Science

SIMON FRASER UNIVERSITY

Summer 2010

APPROVAL

Name: **Kambiz Kaheshpour**

Degree: **Master of Applied Science**

Title of Thesis: **Dielectric Elastomers as Potential Actuating Elements of Reconfigurable Antennas**

Examining Committee:

Chair:

Dr. Siamak Arzanpour, P. Eng.
Assistant Professor, School of Engineering Science

Dr. Carlo Menon, P. Eng.
Senior Supervisor
Assistant Professor, School of Engineering Science

Dr. Rodney Vaughan, P. Eng.
Supervisor
Professor, School of Engineering Science

Dr. Ash Parameswaran, P. Eng.
Internal Examiner
Professor, School of Engineering Science

Date Defended/Approved: 28/05/2010

Declaration of Partial Copyright Licence

ABSTRACT

This thesis focuses on the design, modeling, fabrication, and testing a planar dielectric elastomer. The planar elastomer is used as an actuator for a novel pattern reconfigurable antenna. The antenna system consists of a monopole, ground plane, and a pair of counter-rotating V-shaped parasitic elements. A simplified mechanical analytical model, validated by simulation performed with software based on the finite element method, is developed to design the actuator. The dielectric elastomer is fabricated by using a three-component silicone, commercially available as TC-5005. Two carbon fiber-reinforced plastic hinges are used to fix the two V-shaped parasitic elements to the dielectric elastomer. The planar movement of the elastomer results on counter-rotating the parasitic elements. Mechanical tests are performed to validate the design and modeling of the actuator. Preliminary tests are carried out to assess potential performance of the proposed pattern reconfigurable antenna.

Keywords: Planar dielectric elastomer; mechanically configurable antenna; finite element method; parasitic element
.

DEDICATION

To my beloved family:

If I could show you how much your presence in my life means to me, the simple phrase of ‘thank you’ would pale and diminish in the sheer enormity of the gratitude I owe.

ACKNOWLEDGEMENTS

I would like to thank my committee members and my colleagues in the MENRVA research group.

TABLE OF CONTENTS

LIST OF FIGURES

LIST OF TABLES

LIST OF ACRONYMS

CFRP	Carbon Fiber Reinforced Plastic
EAP	Electroactive Polymer
DE	Dielectric Elastomer
DEA	Dielectric Elastomer Actuator
DC	Direct Current
DOF	Degree of Freedom
FEA	Finite Element Analysis
FEM	Finite Element Method
GP	Ground-Plane
HFSS	High Frequency Structural Simulator
HS	Hinge Structure
HV	High Voltage
MCA	Mechanically Configurable Antenna
PE	Parasitic Element
RP	Radiation Patten

LIST OF SYMBOLS

P	Electrostatic pressure
ϵ_0	Permittivity of the free space (8.85×10^{-12} F/m)
ϵ_r	Relative dielectric constant of the DE film
V	Applied voltage to the electrodes
z	Thickness of the DE film
C	Capacitance
A	Area of the capacitor plates
E_f	Induced electric filed
U	Stored energy in the capacitor
E	Young's module
ν	Poisson ratio
n	Uniaxial prestretch ratio along the DEA length
Δl	Applied displacement to the DEA along x-direction
Δx^a	Active displacement of the DEA along x-direction
Δy^a	Active displacement of the DEA along y-direction
Δz^a	Active displacement of the DEA along z-direction
l^r	Total relaxed length of the DE
x^r_e	Relaxed length of the DEA
x^r_s	Relaxed length of the uncoated DE
x^p_e	Prestrained length of the DEA
x^p_s	Prestrained length of the uncoated DE
x^a_e	Length of the DEA under activation
x^a_s	Active length of the uncoated DE
y^r_e	Relaxed width of the DEA
y^p_e	Prestrained width of the DEA
y^a_e	Width of the DEA under activation
z^p_e	Prestrained thickness of the DEA

z^a_e	Thickness of the DEA under activation
ε^p_{ii}	Normal components of the (pre)strain, *i*= *x, y, z* directions
ε^a_{ii}	Normal components of the DEA active strain, *i*= *x, y, z* directions
$\varepsilon^a_{xx,s}$	Contractile strain of the uncoated DE under activation
σ^p_{xx}	Generated constant preload as a result of the applied prestrain
σ^a_{xx}	Active stress in the opposite σ^p_{xx} direction reducing the preload
α	Displacing angle of the HS
l_i	HS links *i=1, 2, 3, 4*
J_i	HS revolute joints *i=1, 2, 3*
β	Slant angle of PE
γ	Angle between the PE arms (V-angle)
χ	Electrode length-to-uncoated DE length ratio

1: INTRODUCTION

1.1 Configurable Antennas

The ongoing developments in wireless communications have created a demand for configurable antennas. Such antennas can dynamically configure their far-field radiation pattern (RP) in order to adapt to varying operating conditions [1, 2, 4]. The reconfiguration improves the power efficiency of the transmitted signal over multipath propagation [1, 3]. Consequently, the signal-to-noise ratio enhances and the link reliability improves [1, 4]. The majority of the conventional techniques dealing with configurable antennas depend upon high-cost circuitry associated with complex signal processing [2, 4].

Recently developed antennas using switched parasitic elements (PE) have slightly reduced the cost and complexity. The antenna beam is controlled by changing the reactive loadings on wire PEs near the antenna. Such antenna configurations are potentially useful for beam steering in wide angle multi-path for low-pattern directivity applications. However, the implementation of the antenna array acquires the use of solid-state switches, which might generate nonlinearities [4, 6]. This can degrade the communication performance on the receive or transmit signal [4].

Some innovative approaches have overcome this drawback by mechanically rotating the wire PEs instead of changing their reactive loadings. Such antennas are known as mechanically configurable antennas (MCA) [2, 5,

6]. The mechanical movement of the PEs is used to control the antenna beam by changing the combination of spatial components of the radiating signal [2]. The variation of the beam over a multi-path propagation offers an angular diversity action [1, 6]. However, the PE movements may introduce long-deposed mechanical reliability issues. On the other hand, controlling the PE motions requires an actuating hardware, power supply, and control electronics.

The MCA's performance is comparatively slow, and do not have the beam forming ability or power handling capabilities for an array with similar volume of the conventional techniques [2, 5, 6]. The changes are applied to the physical antenna structure, thus, continuous reconfiguration schemes of MCAs may not be possible by other modalities [6].

1.2 Motivation

1.2.1 MCA Configuration Using a Pair of Rotating-PE [6]

Fig. (1-1) demonstrates a schematic model of a MCA. The antenna system is comprised of a monopole antenna at a center of a finite ground-plane (GP) and a pair of rotating V-shaped wire PEs. The PE symmetrical orientation is to reduce the impedance variation of the monopole at the matching frequency, while generating reasonably uncorrelated RPs.

The antenna (active element) with a nominal frequency of $1GHz$ is a quarter-wavelength long. The PEs (passive elements) are each a half-wavelength long. The V-angle, shown by γ, is defined as the angle between the two arms of the PEs, see fig. (1-1a). The slant-angle of the PEs, shown by β, is

defined as the angle between the closer PE arm to the GP and the GP, see fig. (1-1b). The simulation result obtained from the high frequency structural simulator (HFSS) demonstrated the variations of γ and β affects the far-field RP. As the PEs become closer to the antenna their interference with the RP goes higher. In addition, the system requires an actuator to control the PE motion by varying the β. There are two slots implemented on the GP for each PE. Each slot is a tenth-wavelength away from the antenna. Controlling the PE motion has to be done by an actuator through the slots from beneath the GP.

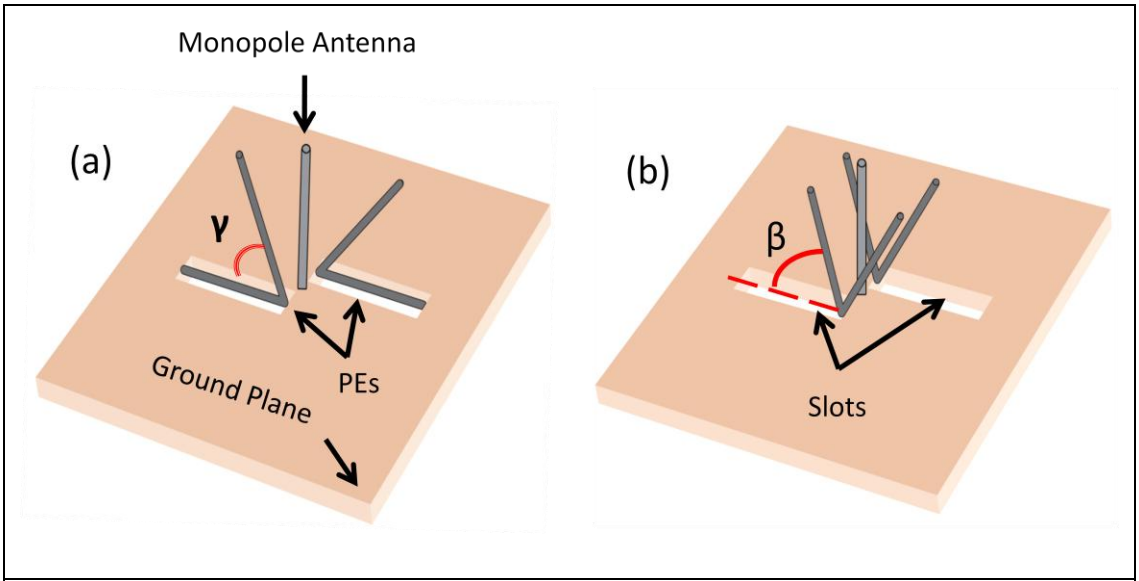

Fig. 1-1 The MCA comprised of a monopole located in the center of a GP, and a pair of counter rotating parasitic elements. The system requires an actuator to rotate the PE. The V-angle and slant-angle of the PEs are respectively shown by γ and β.

1.3 Objective

We propose a novel actuation technique using a dielectric elastomer actuator (DEA) potentially useful for the MCA. DEAs are inherently low cost, produce large deformations [7, 13], have high force-to-weight ratio [9, 13], high force-to-volume ratio [13], and low power consumption (microamperes) [8, 13].

Thus, they present features suitable for MCAs, which could potentially mitigate the MCAs in terms of actuation technology [5].

1.3.1 Actuator Configuration

The proposed actuator is composed of a planar DEA and two hinge structures (HS). The structures are embedded in parallel to each other on the DEA surface, see fig.(1-2). Under activation, the DEA expands along its initial in-plane dimensions. The DEA deformation is transformed to PE counter-rotation via the HS. The rotation angle of the HS is denoted by α. The PEs are bonded to the side of their corresponding hinge.

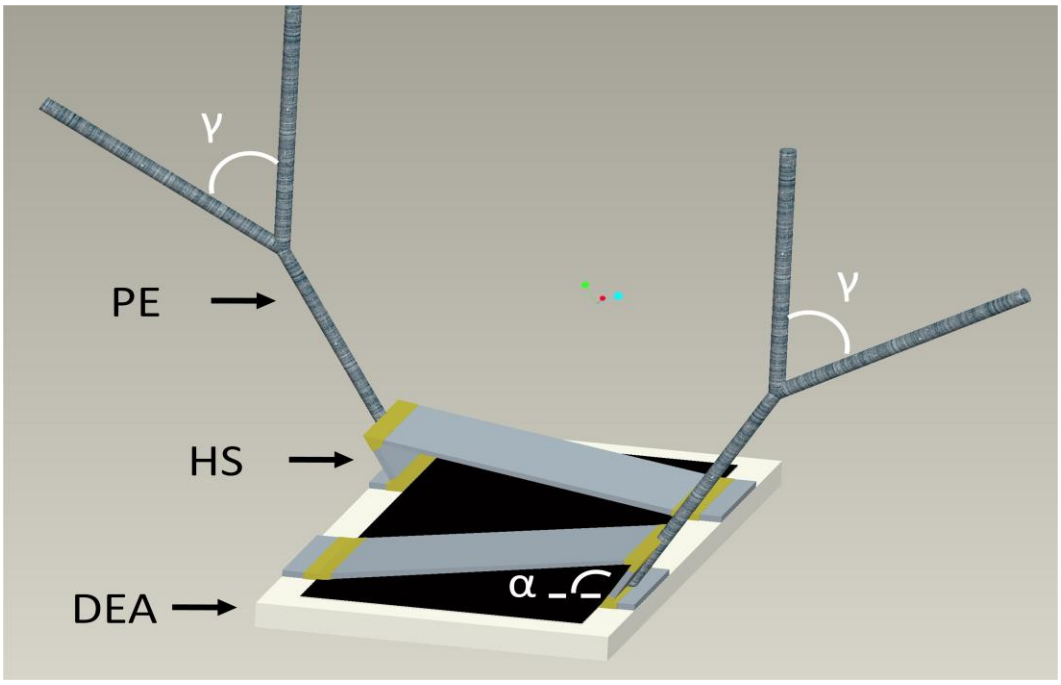

Fig. 1-2 The schematic model of the DEA with proposed configuration. Under activation, the in-plane deformation of the DEA is transformed to counter-rotation of the PEs via HS angular displacement.

The DEA voltage (kilovolts) is supplied by a miniaturized DC-to-high voltage (HV) DC convertor. Due to the HV requirements of the DEA, the mechanism has to be located beneath the GP and electrically isolated from the antenna system.

Prior to fabrication of the prototype, the DEA behavior is modeled analytically. The numerical results are compared with FEM simulations. Using both models (analytical and FEM), the impact of different electrode-to-DE length on the DEA planar deformations is investigated. The relationship between the applied voltage to the DEA and the PE angular displacement is computed.

The DEAs with optimum configurations are fabricated. The physical deformations of the actuator under applied voltages to the DEA are measured. The MCA with a pair of rotating-PE is manufactured and tested in an anechoic chamber. The preliminary physical measurements of pattern variations and reflection coefficients for different PE slant angles are demonstrated.

The rest of the thesis is organized in five additional chapters followed by two appendices.

Ch. 2 In ch.2, a brief literature review related to the electroactive polymers (EAP) in particular DEA is presented. In addition, some examples of existing DEA configurations and their promising applications are selected to provide an overview of the current state of the actuator technology.

Ch.3 In ch.3, the electromechanical performance of the actuator is foreseen through a simplified analytical model. The relationship

between the PE slant angle and the applied voltage to the DEA is described by closed-form solutions.

Ch.4 In ch.4, the DEA planar deformation is numerically estimated by assigning values of the free parameters in solutions. In addition, FEM-based simulations are used to validate the numerical results. Moreover, the impact of the electrode length-to-DE length variations on the DEA deformation is investigated.

Ch.5 In ch.5, the fabrication procedure of the planar DEA is explained. The DEA deformation and PE rotation are physically measured under applied voltages. These results and compared with those numerically computed from the analytical and FEM models. In addition, the preliminary physical measurements of pattern variations and reflection coefficients of the antenna system for different PE slant angles are demonstrated.

Ch.6 In ch.6, the conclusion and future directions are discussed.

Appendix A The generalized Hooke's law of elasticity is given in appendix A.

Appendix B The derivation of the electrostatic pressure for a planar DEA configuration is shown in appendix B.

.

2: ELECTROACTIVE POLYMERS: A LITERATURE REVIEW

2.1 Active Polymers

A polymer is a long chain of repeating structural units, known as monomers, typically connected by covalent chemical bonds [10, 11]. The basic mechanical properties of a polymer such as stiffness, density, durability depends on the characteristics of its intrinsic monomers, and the cross link between the two different chains [10, 12]. Polymers may be passive in nature, but by embedding active materials they can become stimuli-responsive [12]. There are many types of active polymers with different controllable properties, due to a variety of stimuli. Depending on the type of actuation, they are generally categorized as non-electrically deformable polymers (driven by nonelectric stimuli such as light, temperature, pH, *etc*.) and electro-active polymers (driven by electric inputs) [12, 13].

2.2 Electroactive Polymers (EAP)

Electro-active polymers refer to a class of polymers, which undergo a size and/or shape change when subject to electrical stimulation (i.e. voltage or current) [14, 15]. Depending on the operation principle, these materials classify into two major categories: ionic and electronic [14, 15]. The qualitative comparison of the properties of ionic and electronic EAPs is given in table (2-1).

2.2.1 Ionic EAPs

Ionic EAPs change shape by displacement or diffusion of ions [16]. Under applied electric fields, ions generally distribute across a wet or solid electrolyte and consequently provoke an electromechanical change in the configuration of the materials [12, 16]. Ionic EAPs have strong bending capabilities, which are driven by few volts [8, 12, 16]. Typically, their response time is low (tenth of a second) and their relaxation time is approximately a few minutes [8, 13]. Ionic EAPs include [8, 13]: carbon nanotubes, polymer-metal composite, polyelectrolyte gels , and conducting polymers.

2.2.2 Electronic EAPs

Electronic EAPs induce large displacements, which are driven by coulomb forces [13, 14, 17]. Typically, they present a rapid response (milliseconds) and a low relaxation time (few seconds) [8, 13, 18]. These materials have high mechanical energy density, require high activation fields (>10 V/μm), and can operate in a dry state with no major constraints [14]. Some examples of the electronic EAPs include [8, 13, 14]: dielectric elastomers (DEs), electrostrictive graft elastomers, piezoelectric polymers, ferroelectric polymers, and liquid crystal elastomers.

	Ionic	Electronic
Type	Mostly bending actuators with strong bending ability	Planar actuators with large in-plane deformations
Operational condition	Require electrolyte (wet condition)	Also work in dry condition
Activation Voltage	Low voltage (few volts)	High voltage (several kilovolts)
Response time	Slow response (tenth of a second), slow relaxation (few minutes)	Rapid response (millisecond) relaxation (seconds)
Active Stress	Fairley low activation stresses	Fairley large activation stresses
Long-term stability	Production of stable materials/actuators is difficult	Long life under ambient condition
components	Expensive	Low-cost

Table 2-1 Qualitative comparison of properties of ionic and electronic EAPs [8]

2.3 Dielectric Elastomer Actuator (DEA)

Among the EAPs, the DEAs have shown unique strain potential and relatively good electromechanical performance, which have received increased attention over past few years [9, 21].

In principle, DEA is a compliant capacitor, made of an elastic polymer for dielectric and compliant conductive coatings for electrodes [14]. The actuator technology is based on induced electric field deformation. Once the capacitor is electrically charged with high DC voltage (several kilovolts), the attraction between the opposing charges of the electrodes squeeze the DE film in the

direction of generated electric field [13, 14]. Consequently, the compliant film contracts in thickness direction and expands in its in-plane dimensions, see fig. (2-1). The repelling forces between equal charges on the two electrodes help the in-plane expansion of the DE [13, 14]. The electrostatic pressure P, also known as Maxwell stress, acting on the DE can be calculated for given applied voltage V and dielectric thickness z as given in eq. (2-1) [14].

$$P = \varepsilon_o \varepsilon_r (\frac{V}{z})^2 \qquad (2\text{-}1)$$

where, ε_0 is the vaccuum permitivitty equal to $8.85\times10^{-12} F/m$, ε_r is the relative dielectric constant. The derivation of the eq. (2-1) is given in Appendix B.

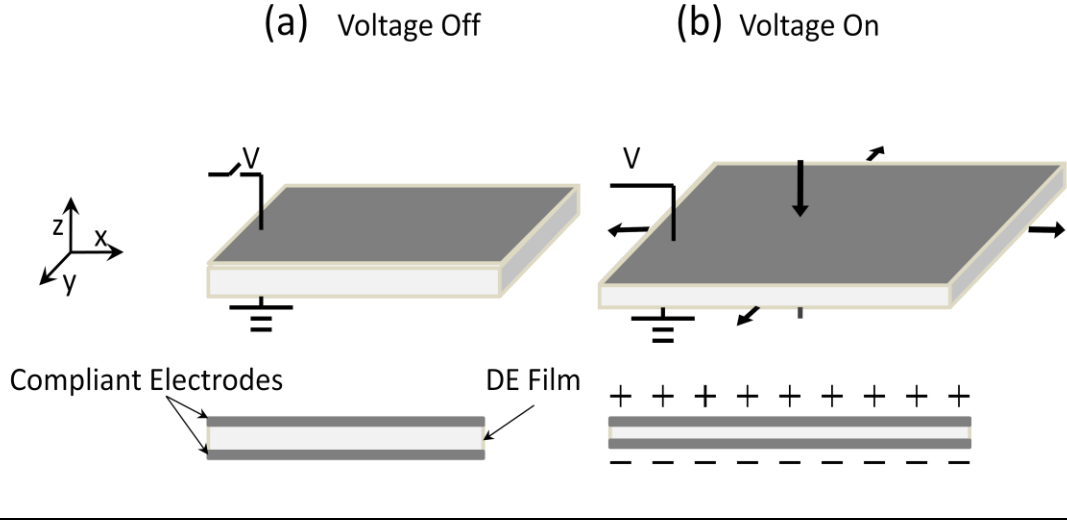

Fig. 2-1 Operation principle of a DEA unit

Given the elasticity of the film, the flexible capacitor returns to its initial state when the voltage is switched-off, and the capacitor is discharged. Thus, the

electromechanical coupling transforms the stored electrical energy of the capacitor directly to mechanical work, by producing large strains [19, 20].

2.4 Existing DEA Configurations

To this date, different configurations of DEAs have demonstrated their capabilities for various applications. Some selected configurations are presented in the following sections to provide an overview of the state of technology related to the actuator type.

2.4.1 Stack Actuator [24, 25]

DEs are stacked in several layers with compliant electrodes embedded in between each layer. During the activation, the stack contracts in DE thickness direction. Therefore, the mechanism functions as a linear actuator. The configuration handles primarily external pressure forces in the thickness direction of the film. Under external tensile forces, the electrodes have to transmit the related tensile stresses between the DE film layers. The reported strains and stresses for this configuration were up to 15% and $20N/mm^2$.

2.4.2 Folded Actuator [24, 25]

The DEA folded configuration is analogous to the stack actuator. Instead of stacking many distinct layers of DE film, a design is possible by folding a single DE film continuously coated with electrodes on both sides. The reported contractile strains along the thickness direction of the elastomer film were up to 15%.

2.4.3 Helical Actuator [24, 25]

Recently, a new configuration of a DEA with helical shape was presented. It consists of a two helically wound DE layers with alternating electrodes.

2.4.4 Unimorph and Biomorph Actuators [14, 29]

The unimorph actuator is a bending actuator. A DEA is constrained on one side, and only bends from the initial in-plane position towards the constraining layer.

The biomorph actuator is a bending/elongation actuator, where at least two layers of DE films are stacked on top of each other. Either an elongation (under activation of both layers), or bending-deformation (under activation of only one layer) is obtained. Unlike to the unimorph, the biomorph actuator is able to bend back and forth from the initial in-plane position.

2.4.5 Diaphragm Actuator [26-28]

The DEA is stretched onto a rigid frame. An applied gas pressure in to the hole from one side of the membrane forces the film to bulge out. Under activation, the membrane relaxes and deforms further outwards. The reported out-of-plane displacements were up to 50% of the membrane diameter, and the pumps were demonstrated with a flow rate of $30-40mL/\min$ at $2.5kPa$. The potential applications of this configuration are loudspeakers or blood pumps.

2.4.6 Diamond-shaped Actuator [30]

The diamond-shaped actuator is a linear actuator composed of a pre-stretched DEA fixed in a four bar linkage structure. In addition, a pair of elastic bands attached parallel to each two adjacent bars generates the prestretch load. Under activation, the film relaxes thus the actuator to elongate in one direction.

2.4.7 Balloon-shape Actuator [31]

A DEA with a spherical shape is inflated with compressed air. The compressed air introduces a uniformly distributed pressure force perpendicular to the inner surface of the active layer. The balloon was significantly prestrained during the inflation to reach the desired thickness of the film. Under activation the balloon expanded in volume. Simultaneously, the inner pressure of the actuator reduced according to the compressibility behavior of the utilized gas. The expansion of the balloon was not uniform in all the directions, and there were generated active localized expansions. Physical measurements of the preliminary prototype reported a deformation of 2.3% when compressed by $30N$ under radial directions.

2.4.8 Rolled Actuator [14, 32-34]

The DEA is prestrained biaxially, and wounded around a compressed spring coil. The DEA expands along its axial direction under activation. The induced strains of 35%, and blocking forces of up to $20N$ were reported. Segmenting the electrodes into several individual active regions allows the actuator to bend. The possible application of rolled actuators falls in the field of prosthetics due to their

high energy density and their noiseless operation. Thus, rolled actuators often referred as “artificial muscles” due to their muscle like behavior.

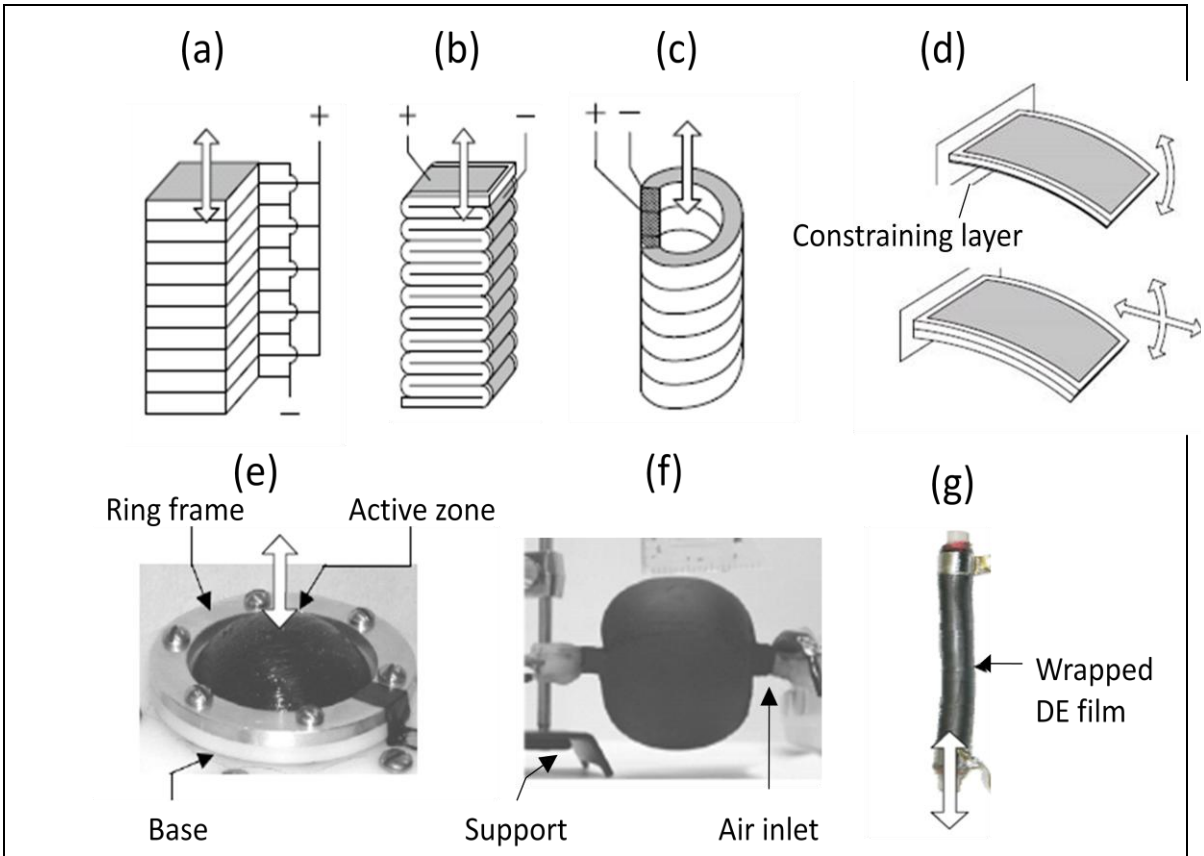

Fig. 2-2 (a) stack actuator (b) folded actuator (c) helical actuator (d) unimorph (top) and biomorph (down) actuators (e) diaphragm actuator (f) balloon actuator (g) rolled actuator

2.5 DEA’s Potential Applications

So far, several DEA configurations have been proposed including stack, bending, roll actuators, etc. The majority of the configurations are capable of producing linear elongation, or uniaxial bending deformation. Due to their distinctive strain capabilities and unique electromechanical performance, such actuators have potential applications in variety of disciplines such as robotic prosthesis, rehabilitation systems, anthropomorphic robots, legged robots, as

well as space, antennas, and toys [21, 32, 35-37]. Some examples of DEA promising applications are presented in the following sections.

2.5.1 Fish Robot [38]

Recently, researchers at MIT have developed a simplified fish robot 8 inches long, compromising of 10 components. The fish robot mimics the swimming of trout and bass. The novel design uses soft polymers as active materials with graded mechanical stiffness. The individually activated segments are located in the tail and the section that tail meets the body. The DEA contraction on either side of the body generates a wave-like motion flowing from head to tail. This undulant propulsion allows the robot fish to swim more naturally. The prototype requires $2.5-5 Watts$ of power currently provided from an external source.

2.5.2 Martian Jumping Rover [39, 40]

A research study proposed by the European Space Agency (ESA) confirms the promising technology of DEA-based actuator for a robotic locomotion system. The system is considered as an elastic spherical rover with diameter of 2m with an internal active mechanism for vertical jumping. In addition, the wind energy is supposed facilitate the surface motion of system. The active mechanism of the rover is assumed to be a cylindrical bar placed inside the sphere equipped with hollow cylindrical DEA. Under activation, the DEA contracts axially, and expands radially. The jumping mechanism could potentially raise either the center or the bottom points of the rover. The simulation

results reveal jumping of obstacle heights corresponding to more than 7% of the diameter of the rover. The model still lacks the design of the electronics with specific requirements of power, size and mass, as well as the identification of proper operational procedures.

2.5.3 Linear Peristaltic Pumps [36, 41]

A research study reports a novel bio-inspired concept for development of linear peristaltic pumps for incompressible fluids. The actuation technology mimics the muscular peristalsis of the biological digestive apparatus. The system is described by a sequence of flexible tubular modules, each comprised of hallow cylindrical DEAs. The DEA operates in entirely radial form. The sequential activation of individual modules allows the fluid inlet. The transduction performance of the system is foreseen through an analytical model based on linear elasticity. The solutions were compared with those provided by FEM. The analytical and simulation models were verified by comparison with the experimental measurements obtained from a preliminary prototype. Nonetheless, the concept is still under laboratory investigation.

2.5.4 Tuneable Dielectric Resonator Antenna [5]

A feasibility study investigates a direct tuning of the antenna through voltage-controlled deformation of a dielectric resonator. The antenna impedance and tuning depends on the shape of the dielectric. The thickness variation of the polymeric medium (the antenna or a component of the antenna) is controlled by means of a DEA for dielectric. A compliant cylindrical dielectric resonator

deforms to change the radius-to-height ratio in order to change the resonant frequency of the antenna. The volume of the deformable DRA is constant. Therefore, as consequence of the radial expansion, the height decreases. The prototype is comprised of a circular DEA stretched on a circular rigid frame. The system is preloaded by means of four loaded micro-scale spring cantilevers placed between the DEA and the frame. The simulation results demonstrate the far-field RP variations for different aspect ratios and resonant frequencies. This study shows the promising properties of EAPs for smart antenna applications. Nevertheless, optimal designs are requisite for an efficient and robust implementation of the system.

2.5.5 Anthropomorphic Skeleton of an Upper Limb [16, 35, 42]

A preliminary research study illustrates the application of contractile DEAs as pseudo-muscular apparatus for the actuation of an anthropomorphic skeleton of an upper limb. The model is comprised of two rods, hinged with disregarded friction. The extremities of the contractile DEA are connected to the rods with additional hinges. The DEA consists of two helically wound layers of DE with alternating electrodes. The contraction of the actuator facilitates the forearm rotation against its weight. The preliminary data reports contraction strain of about -3% in response to a driving field of $15V/\mu m$. Nonetheless, higher performances are foreseen with future improvements in DEA technology.

2.6 Conventional vs. EAP-based Actuators

Conventional actuators include hydraulic, pneumatic (cylinders), and electrical/electromechanical actuators (motors and switches). The advantages and drawbacks of these technologies are shown in table (2-2).

The main drawback of the conventional actuators is that either the actuator itself or energy supplies or transmission lines are bulky and heavy. In addition, the conventional actuators have poor performance due to physical scaling effects, and fabrication difficulties [44, 45]. This is particularly unfavorable when it comes to applications where small mass or volume-specific performance is necessary. When it comes to active structures, working with conventional actuators would typically end up with a complex framework structure where all the degrees of freedom (DOF) have to be controlled [8].

Unlike the conventional actuators, the EAP-based actuators are mechanically simple and do not consist of many interacting parts [13]. Using EAPs, the separation between the structure and the deriving actuator is not required. Thus, they are suitable for development of electromechanical devices with no gears, bearings, or other complex mechanism [43]; this is an advantage in terms of cost and performance. Moreover, EAPs tend to be lightweight, and simpler to integrate into the systems [19]. They could potentially replace the rigid mechanical devices with better performance. Yet, their current limitations such as low actuation force and robustness have confined the scope of their practical applications [18, 19, 46].

Type	Advantages	limitations
Hydraulic	Generation of linear and rotator motions, high payloads, reliable system, deliver great power, high stiffness, fast response, high frequencies, low-noise, self-lubricating	Difficult to control, viscosity of oil changes with temperature, leaking is dangers, flammable fluid
Pneumatic	Light-weight, small-size, complaint system, high payload-to-weight ratio, no return lines for fluids needed, clean system, fluid inflammable	Lower forces capabilities due lower pressures, lower efficiency since is not self-lubricating
Electric	Large verity of possible devices (AC, DC, induction, stepper motors), smaller power supplies, simple transmission line from supply to device	Generation of small torques in relation to their size and weight

Table 2-2 Advantages and drawbacks of the conventional actuator technologies [8]

3: MODELING

3.1 Actuator Configuration

We use a planar DEA as an actuating element of a MCA to displace a pair of V-shaped wire PEs in vicinity of an antenna. Subsequently, change the antenna far-field RP. The actuator is comprised of a planar DEA and two hinge structures (HS). The structures are embedded in parallel to each other on the DEA surface, see fig. (3-1). The PEs are glued to the side of their corresponding hinge.

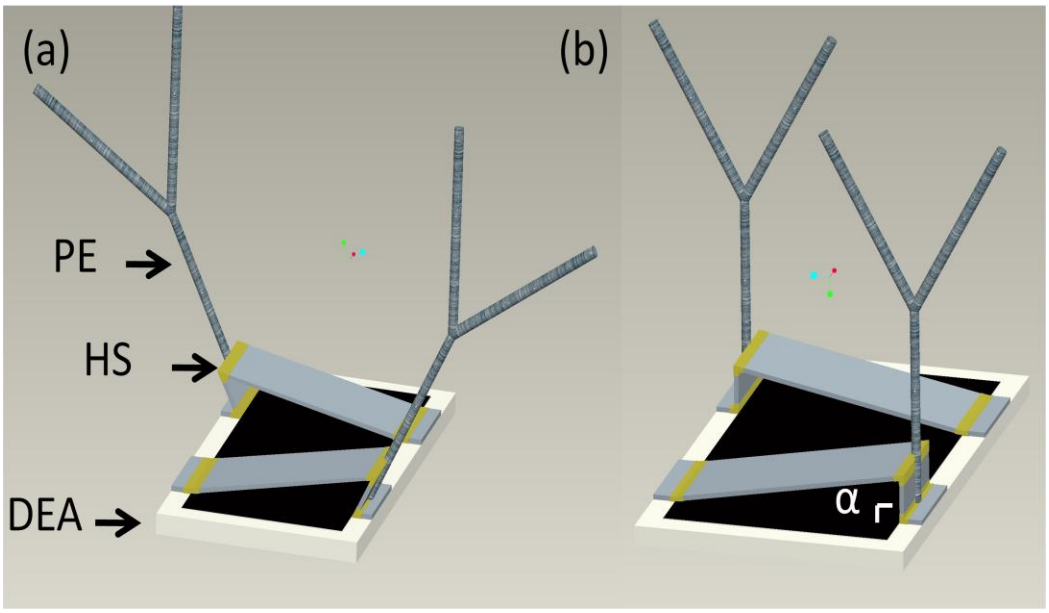

Fig. 3-1 The schematic model of the DEA with embedded hinges. Under activation the in-plane deformation of the DEA is transformed to the counter-rotation of the PEs. (a) DEA is relaxed (b) DEA is activated.

Under activation, the DEA expands along its initial in-plane dimensions. The DEA linear deformation is transformed to PE counter-rotation via the HS. The rotation angle of the HS is denoted by α, see fig. (3-1b). The voltage (several kilovolts) is supplied by a miniaturized DC-to-high voltage (HV) DC convertor.

3.2 Planar DEA

The planar DEA is uniaxially prestretched, along is initial length, and fixed on both ends. In general, prestretching increases the electrical breakdown strength [8, 47], avoids pull-in failures [8], and reduces the required voltage to obtain the same electrostatic pressure [8, 13, 47]. As shown in fig. (3-2), the DE film is not continuously coated with electrodes on top and bottom. Thus, the uncoated segments would react as preloaded elastomeric springs pulling the materials, once the film is stretched. Under activation, the DEA in-plane expansion reduces the preload tension. Simultaneously, the materials relax and further deform in particular in prestretch direction.

Constant prestretch ratios are obtained by clamping the stretched DE film on both sides along the DEA length. The effect of the generated preloads on the DEA active displacements is investigated.

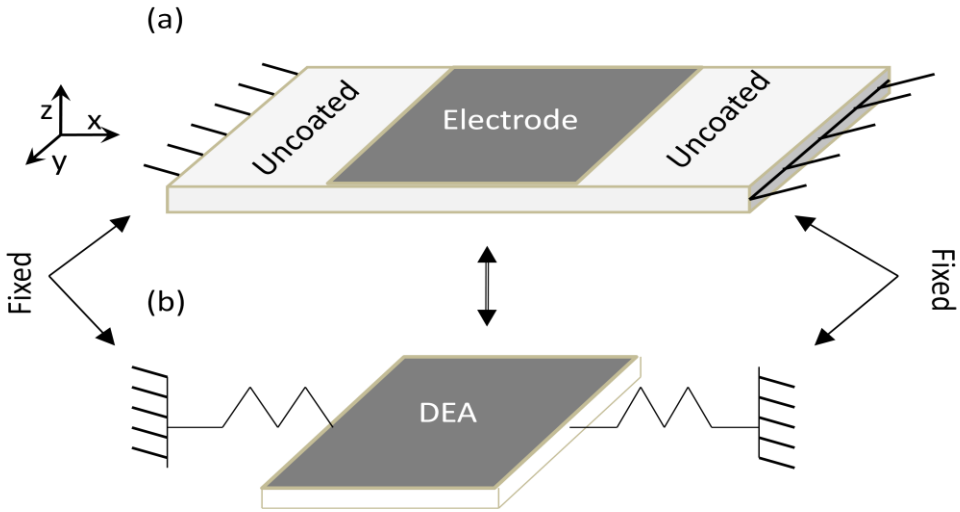

Fig. 3-2 Schematic model of the planar DEA, while held in prestretch. The uncoated DE segment is modeled as a preloaded mono-dimensional spring, which facilitates the deformation of the DEA under activation.

3.2.1 Modeling Simplifications

The term 'system model', often relates to a mathematical representation formulated to simulate and predict behavior of a physical system [8, 13, 15, 22]. An analytical model is an ideal abstraction of the physical reality, by which the complexity of the physical system could be reduced. For instance, the materials that are hyperelastic [13] in reality are chosen to be modeled as linear elastic materials for simplicity. Linear models do not cover the hyperelastic behaviors of the materials for large strains. However, linear models are useful in order to foresee the hyperelastic behaviours. Therefore, having a linear model that describes to some extent the hyperelastic bahavior of the elastomer is an essential elementary modeling step of the DEA. Moreover, to mathematically describe the electromechanical coupling of the system we made the following simplifications:

- The materials are assumed to be linearly elastic. Thus, the components of the stress are linearly proportional to the components of the strain acting on the elastomer [10, 49].
- The materials are assumed to quickly recover their initial state of stable equilibrium after being deformed by an external force. Therefore, it is possible to derive a time-independent model, which relates the strains and stresses acting on the elastomer [10, 49].
- The DEA unit is modeled as a single cuboid element (able to deform in three dimensions). The uncoated DE segments are modeled as mono-dimensional springs attached to either sides of the DEA, see fig. (3-2).
- We are interested in the macroscopic deformations of the DEA. For this purpose, the strains are defined as $\varepsilon = \frac{\Delta l}{l}$, where Δl corresponds to the macroscopic deformation of the entire DEA unit along its length.
- All the shear effects are neglected as the DEA is supposed to be connected to a mono-dimensional pulling spring.
- The materials are assumed to be isotropic, thus their mechanical properties i.e. Young's module E and Poisson ratio ν are the same in all directions [10].
- The cubical geometry of the elastomer is preserved under deformation, and no wrinkling effects are permitted [8, 13].

- The electromechanical coupling is obtained by introducing an equivalent electrode pressure in the thickness direction of the film [14, 20].
- The change in DEA volume is zero under applied external load force [13] .

3.2.2 Geometry and Boundary Conditions

The geometry, force distribution, and applied constraints are symmetrical at mechanical equilibrium, fig. (3-3). Thus, static stress-strain analysis is performed on one quarter of the model geometry.

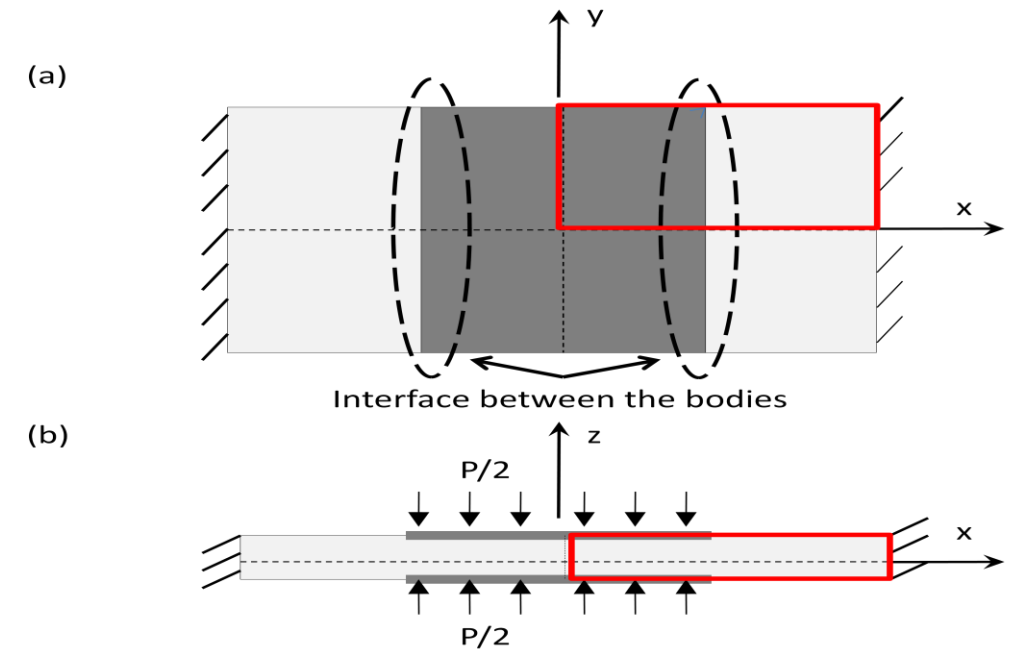

Fig. 3-3 The dark gray and light gray segments respectively correspond to the electrodes and the uncoated DE. The geometry, force distribution, and the applied constraints are symmetrical at mechanical equilibrium. The FEA is performed over a quarter of the geometry.

The parameters of the system, such as the dimensions (x, y, z), are denoted by superscripts $'r'$, $'p'$, and $'a'$ for the relaxed, prestrained, and activation states. In

addition, subscripts 'e' and 's' respectively indicate the DEA and the uncoated DE segments (springs), see fig. (3-2).

3.2.3 Uniaxial Prestrain

It is assumed that the DE is prestretched n-times $(n \geq 1)$ by its initial length l^r along the x-direction for the total displacement of Δl, and fixed on both sides. The prestrained length of the film is denoted by l^p. Thus:

$$\Delta l = l^p - l^r = nl^r - l^r = (n-1)l^r \tag{3-1}$$

The applied strain to the DE along the $x-$direction ε_{xx}^p is defined as the ratio of the applied displacement to the total relaxed length of the DE. Hence,

$$\varepsilon_{xx}^p = \frac{\Delta l}{l^r} = n-1 \tag{3-2}$$

Reducing the Hooke's law (Appendix A) by removing the shear components of the stress-strain, the constant preload stress σ_{xx}^p generated as the result of the applied strain ε_{xx}^p along the x-direction is calculated as:

$$\begin{bmatrix} n-1 \\ \varepsilon_{yy} \\ \varepsilon_{zz} \end{bmatrix} = \frac{1}{E}\begin{bmatrix} 1 & -\nu & -\nu \\ -\nu & 1 & -\nu \\ -\nu & -\nu & 1 \end{bmatrix}\begin{bmatrix} \sigma_{xx}^p \\ 0 \\ 0 \end{bmatrix} \tag{3-3}$$

Hence,

$$\sigma_{xx}^p = E(n-1) \tag{3-4}$$

At this state, there are no external pressures acting on the bodies along $y-$ and $z-$directions, thus, the normal components of the stress σ_{yy} and σ_{zz} are zero.

When the elastic materials are pulled in one direction, they become thinner in the other two directions. Therefore, ε_{yy}^{p} and ε_{zz}^{p} can be written in terms as of applied the uniaxial strain ε_{xx}^{p}.

$$\varepsilon_{yy}^{p} = \varepsilon_{zz}^{p} = -\nu\varepsilon_{xx}^{p} = -\nu(n-1) \tag{3-5}$$

Therefore, the DEA prestrained dimensions, and the length of the preloaded spring can be calculated as the function of the applied uniaxial prestrain ε_{xx}^{p} and the relaxed dimensions of the system. Hence,

$$\begin{aligned} x_s^p &= x_s^r(\varepsilon_{xx}^p + 1) \\ x_e^p &= x_e^r(\varepsilon_{xx}^p + 1) \\ y_e^p &= y_e^r(-\nu\varepsilon_{xx}^p + 1) \\ z_e^p &= z_e^r(-\nu\varepsilon_{xx}^p + 1) \end{aligned} \tag{3-6}- (3-9)$$

3.2.4 Activation

The equivalent electrostatic pressure (appendix B) is mechanically applied to the top surface of the DEA acting along the thickness direction. Thus, the DEA expands by Δx^a and Δy^a along $x-$ and $y-$directions, and contracts by Δz^a along the $z-$direction as shown in fig. (3-4). Therefore, the induced displacements are defined with respect to the initial dimensions of the DEA at prestrained state, as given in equations (3-10)-(3-12):

$$\begin{aligned} \Delta x^a &= x_e^a - x_e^p \\ \Delta y^a &= y_e^a - y_e^p \\ \Delta z^a &= z_e^a - z_e^p \end{aligned} \tag{3-10}- (3-12)$$

Respectively, the normal components of the active strain ε_{xx}^{a}, ε_{yy}^{a} and ε_{zz}^{a} are defined as the ratio of the active displacements Δx_e^a, Δy_e^a, and Δz_e^a to the prestrained dimensions of the DEA.

$$\varepsilon_{xx}^{a} = \frac{\Delta x^{a}}{x_e^{p}}, \qquad \varepsilon_{yy}^{a} = \frac{\Delta y^{a}}{y_e^{p}}, \qquad \varepsilon_{zz}^{a} = \frac{\Delta z^{a}}{z_e^{p}} \qquad \text{(3-13)- (3-15)}$$

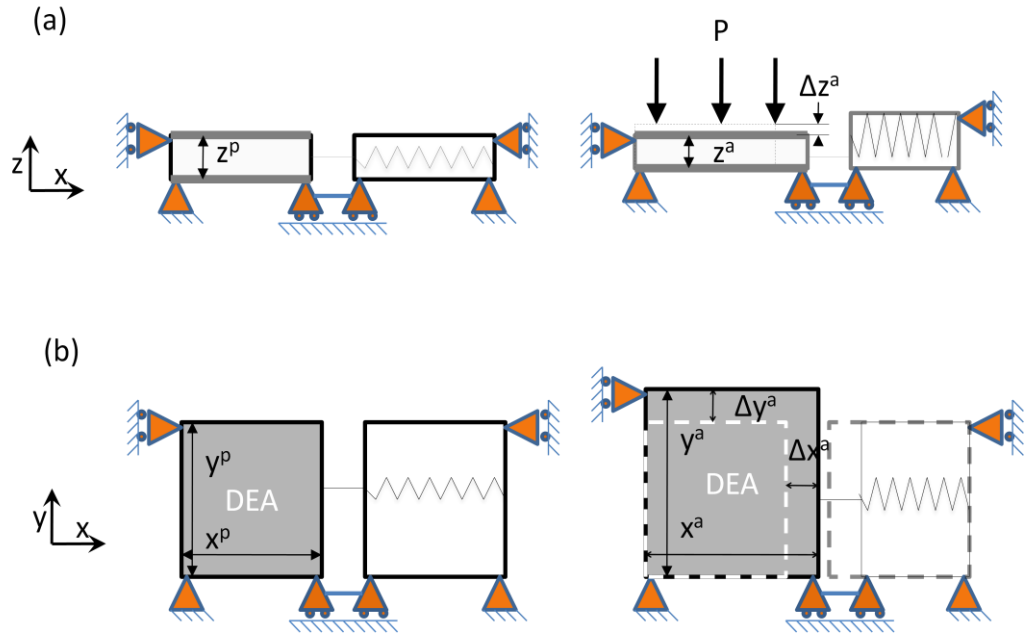

Fig. 3-4 Schematic of the DEA quarter-model under applied pressure. The shear forces are neglected. There is a roller at the interface between the two bodies. The expansion of the DEA forces the spring to contract by Δx^a, and simultaneously reduces the preload.

The goal is to solve for the variable x_e^a in terms of the applied voltage. This variable relates to the reference point defined exactly on interface between the DEA and the elastomeric spring. The DEA expansion forces the spring to contract by the mount of Δx^a to reduce the preload stress σ_{xx}^{p}. The total length of the system is always fixed. The contractile strain of the spring denoted by $\varepsilon_{xx,s}^{a}$ is

therefore defined as the ratio of the contractile displacement to the initial length of the spring.

$$\varepsilon_{xx,s}^{a} = \frac{-\Delta x^{a}}{x_{s}^{p}} = \frac{-x_{e}^{a} + x_{e}^{p}}{x_{s}^{p}} \tag{3-16}$$

Following the Hooke's law, the active stress σ_{xx}^{a} is proportional to $\varepsilon_{xx,s}^{a}$, and reacts in the opposite direction of σ_{xx}^{p} to reduce the preload.

$$\sigma_{xx}^{a} = E\varepsilon_{xx,s}^{a} = E(\frac{-x_{e}^{a} + x_{e}^{p}}{x_{s}^{p}}) \tag{3-17}$$

At this state, there are only two components of stress acting on the DEA: the active stress σ_{xx}^{a} in the x-direction and the applied compressive pressure P in the negative $z-$direction. There is no external stress along the $y-$direction, thus, σ_{yy} is zero.

The constitutive relations are:

$$\begin{bmatrix} \varepsilon_{xx}^{a} \\ \varepsilon_{yy}^{a} \\ \varepsilon_{zz}^{a} \end{bmatrix} = \frac{1}{E}\begin{bmatrix} 1 & -\nu & -\nu \\ -\nu & 1 & -\nu \\ -\nu & -\nu & 1 \end{bmatrix}\begin{bmatrix} \sigma_{xx}^{a} \\ 0 \\ -P \end{bmatrix} \tag{3-18}$$

Or equivalently,

$$\begin{aligned} \varepsilon_{xx}^{a} &= \frac{1}{E}\sigma_{xx}^{a} + \frac{\nu}{E}P \\ \varepsilon_{yy}^{a} &= \frac{-\nu}{E}\sigma_{xx}^{a} + \frac{\nu}{E}P \\ \varepsilon_{zz}^{a} &= \frac{-\nu}{E}\sigma_{xx}^{a} - \frac{1}{E}P \end{aligned} \tag{3-19)- (3-21}$$

By substituting the equations (3-10), (3-13), and (3-17) into the eq. (3-18) and solving for x_{e}^{a}, we have:

$$x_e^a = \frac{x_s^p(1+\frac{\nu}{E}P)+x_e^p}{1+\frac{x_s^p}{x_e^p}} \tag{3-22}$$

Thus, the active stress σ_{xx}^a, eq. (3-17), can be written in terms of the pressure P and the lengths of the materials.

$$\sigma_{xx}^a = \frac{-\nu P}{1+\frac{x_s^p}{x_e^p}} \tag{3-23}$$

Finally, from equations (2-1) and (3-23), the normal components of the active strain are computed in terms of the prestrained dimensions of the system, and the applied voltage. Hence,

$$\begin{aligned}
\varepsilon_{xx}^a &= \frac{\nu\varepsilon_0\varepsilon_r}{E}\left(\frac{x_s^p}{x_e^p+x_s^p}\right)(\frac{V}{z_e^p})^2 \\
\varepsilon_{yy}^a &= \frac{\nu(\nu+1)\varepsilon_0\varepsilon_r}{E}(\frac{V}{z_e^p})^2 \\
\varepsilon_{zz}^a &= \frac{(\nu^2+1)\varepsilon_0\varepsilon_r}{E}(\frac{V}{z_e^p})^2
\end{aligned} \tag{3-24)- (3-26}$$

Subsequently, the active displacements are computed as:

$$\begin{aligned}
\Delta x^a &= \frac{\nu\varepsilon_0\varepsilon_r x_e^p}{E}\left(\frac{x_s^p}{x_e^p+x_s^p}\right)\left(\frac{V}{z_e^p}\right)^2 \\
\Delta y^a &= \frac{\nu(\nu+1)\varepsilon_0\varepsilon_r y_e^p}{E}\left(\frac{V}{z_e^p}\right)^2 \\
\Delta z^a &= \frac{(\nu^2+1)\varepsilon_0\varepsilon_r z_e^p}{E}\left(\frac{V}{z_e^p}\right)^2
\end{aligned} \tag{3-27)- (3-29}$$

The closed-form solutions of active displacements, as a function of relaxed dimensions, voltage, and uniaxial prestrain, are computed as:

$$\Delta x^a = \frac{\nu\varepsilon_0\varepsilon_r}{E}\left(\frac{x_s^r}{x_e^r + x_s^r}\right)\left(\frac{V}{z_e^r(-\nu\varepsilon_{xx}^p + 1)}\right)^2\left(x_e^r(\varepsilon_{xx}^p + 1)\right)$$

$$\Delta y^a = \left(\frac{\nu(\nu+1)\varepsilon_0\varepsilon_r}{E}\right)\left(\frac{V}{z_e^r(-\nu\varepsilon_{xx}^p + 1)}\right)^2\left(y_e^r(-\nu\varepsilon_{xx}^p + 1)\right) \qquad \text{(3-30)- (3.-2)}$$

$$\Delta z^a = \left(\frac{(\nu^2+1)\varepsilon_0\varepsilon_r}{E}\right)\left(\frac{V}{z_e^r(-\nu\varepsilon_{xx}^p + 1)}\right)^2\left(z_e^r(-\nu\varepsilon_{xx}^p + 1)\right)$$

3.3 Hinge Structure (HS)

The HS is basically a four-linkage ($l1, l2, l3, l4$) structure with three revolute joints ($J1, J2, J3$), see fig. (3-5). The HS is embedded along the DEA width ($y-$ direction). The $l1$ and $l4$ links are fixed to the DEA surface. Under activation, the active displacement Δy_e^a changes α. Using a simple trigonometry (cosine rule), the relationship between Δy_e^a and α is computed.

$$\angle\alpha = \cos^{-1}\left[\frac{l_3{}^2 - \left(y_e^p + \Delta y^a\right)^2 - l_2{}^2}{-2\, l_2\left(y_e^p + \Delta y^a\right)}\right] \qquad \text{(3-33)}$$

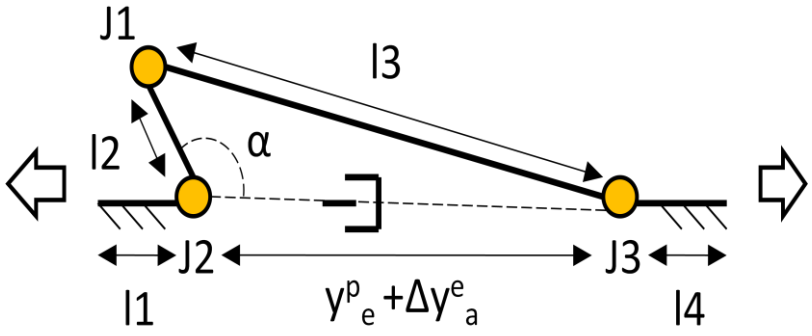

Fig. 3-5 Schematic model of the HS. The structure is composed of 3 revolute joints and 4 links. The active displacement of the DEA changes the rotation angle α.

In the following chapter, we numerically investigate the active deformation of the DEA under applied prestretch ratios by assigning the value of the free parameters. As previously explained, the adapted model tends to be restricted to certain assumptions or conditions (i.e. regular geometries, or simple boundary conditions), and is required to be numerically evaluated by the FEM simulations.

4: NUMERICAL VALIDATION

4.1 Finite Element Method (FEM)

The basic concept of the FEM is the division of the continuous geometry into a set of disjoint elements of simple geometry with finite degrees of freedom (DOF). Each element is characterized as the value of a function or functions at nodal points. The solution is then approximated by connecting or assembling the collection of all elements.

A commercially available FEM based software suitable for structural analysis and solid mechanics is used to perform the finite element analysis (FEA). The software bases the implementation of the stress and strain on the equilibrium equations (4-1)-(4-3) [48], expressed in the global stress components.

$$-\frac{\partial \sigma_{xx}}{\partial x}-\frac{\partial \sigma_{xy}}{\partial y}-\frac{\partial \sigma_{xz}}{\partial z}=F_x \tag{4-1}$$

$$-\frac{\partial \sigma_{xy}}{\partial x}-\frac{\partial \sigma_{yy}}{\partial y}-\frac{\partial \sigma_{yz}}{\partial z}=F_y \tag{4-2}$$

$$-\frac{\partial \sigma_{xz}}{\partial x}-\frac{\partial \sigma_{yz}}{\partial y}-\frac{\partial \sigma_{zz}}{\partial z}=F_z \tag{4-3}$$

where, F defines the volume forces (body forces). In the static analysis, the loads and constrained are fixed in time and has no explicit or implicit time dependencies. Therefore, there is no mass or mass moment of inertia included in the equations.

The FEM implementation of the quarter-model in 3D consists of two cuboids, connected to each other by sharing an interface. Each cuboid is $25\times25mm^2$ with a thickness of $1mm$ representing the DEA and the uncoated DE, see fig. (4-1). The cuboids having identical material properties were modeled as isotropic linear elastic materials. The DE Young's module, E, and the Poisson ratio, ν, were assumed to be $44kPa$ and 0.49 [31].

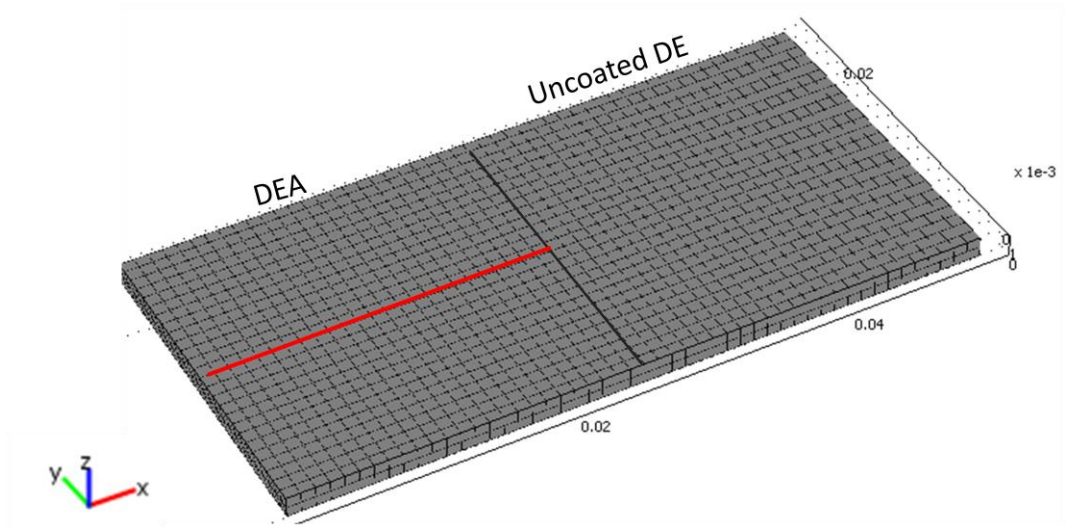

Fig. 4-1 FEM implementation of the quarter model. The cuboid structures represent the DEA (on the left) and the uncoated DE (on the right). The materials were discretized using mapped mesh with square geometry distributed in two separate layers. The data points were selected along the red line on the top surface of the DEA.

The deformation of the bodies under four different prestretch scenarios $(n=1,1.25,1.5,2)$ is investigated. The prestretch ratio, n, defined in the eq. (3-1), corresponds to the ratio of the total pre-stretch length to the total relaxed length of the DE. To create the preload stress along $x-$direction, the system was constrained from one side, and stretched by applying a constant displacement to

the opposite side. For instance, 100% uniaxial prestretch condition $(n=2)$ was attained by applying the displacement of $50mm$ to the length in $x-$direction. In addition, to suppress the rigid body motions, one node was fixed in all directions.

The equivalent electrostatic pressure P was mechanically applied (force/area) to top electrode and acting in the thickness direction. For this reason, the bottom surface of the DEA was constrained in $z-$direction preventing the system to move downwards.

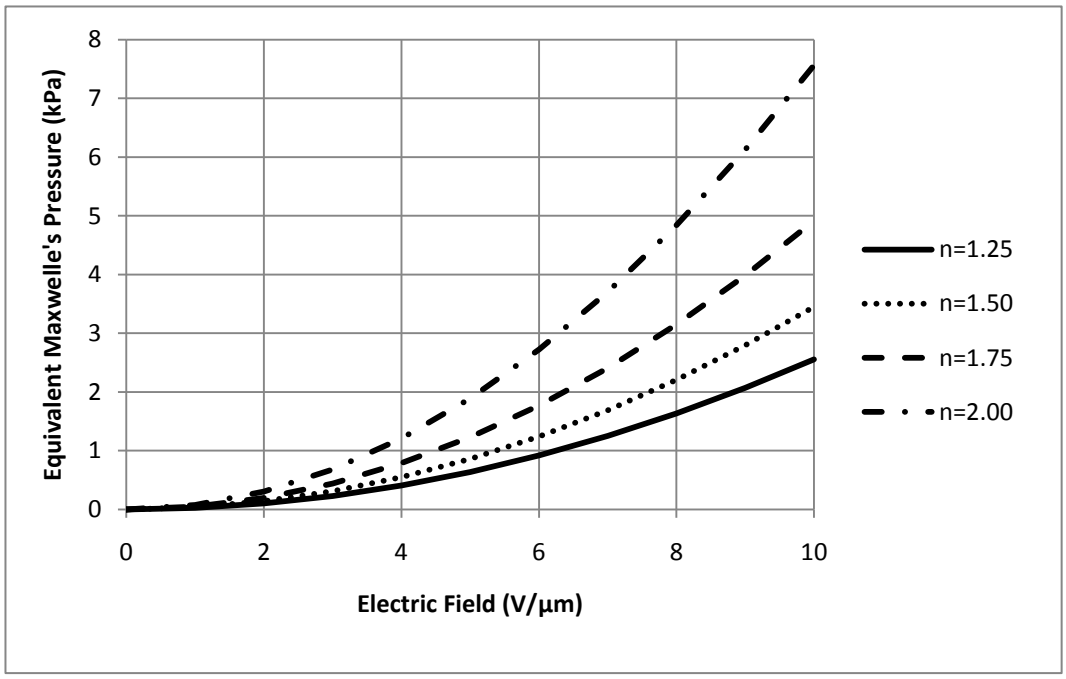

Fig. 4-2 The variations of the applied equivalent electrostatic pressure under applied electric fields for different prestretch ratios.

The equivalent Maxwell's pressure was computed from the eq. (2-1) for the initial thickness z_p^e at each prestrained condition, dielectric constant ε_r of 5, and the applied voltage of up to $10kV$. Fig. (4-2) depicts the variation of the

electrostatic pressure for the four prestretch cases. The variations of the relative dielectric constant were neglected in our calculations.

The model was discretizated using extra-fine mapped-mesh consisting of 5300 square-shape elements, distributed equally in two separate layers, see fig. (4-1). The element size was chosen in such way to acquire the most effective usage of the computing power and to avoid the out-of-memory error arising during post-processing or visualization of the model in mesh-mode.

The active strains were estimated by taking the strain average of 10 points selected along the DEA length in the middle of DEA top surface, see fig. (4-1). Fig. (4-3) depicts the active planar strains of the data points for $n = 2$ prestrained condition. As demonstrated, the distribution of ε_{xx}^{a} and ε_{yy}^{a} are uniform along the DEA length, however, it suddenly drops as becomes closer to the interface boundary between the bodies. This was caused by the shear effects at boundary between the two bodies, which were neglected in the analytical model for simplicity. For this reason, the points under influence of the interface boundary from our calculations were excluded from the calculations. Hence, FEM simulations yielded ε_{xx}^{a} and ε_{yy}^{a} to be approximately 0.04 and 0.1, as the effect of the interface boundary was neglected.

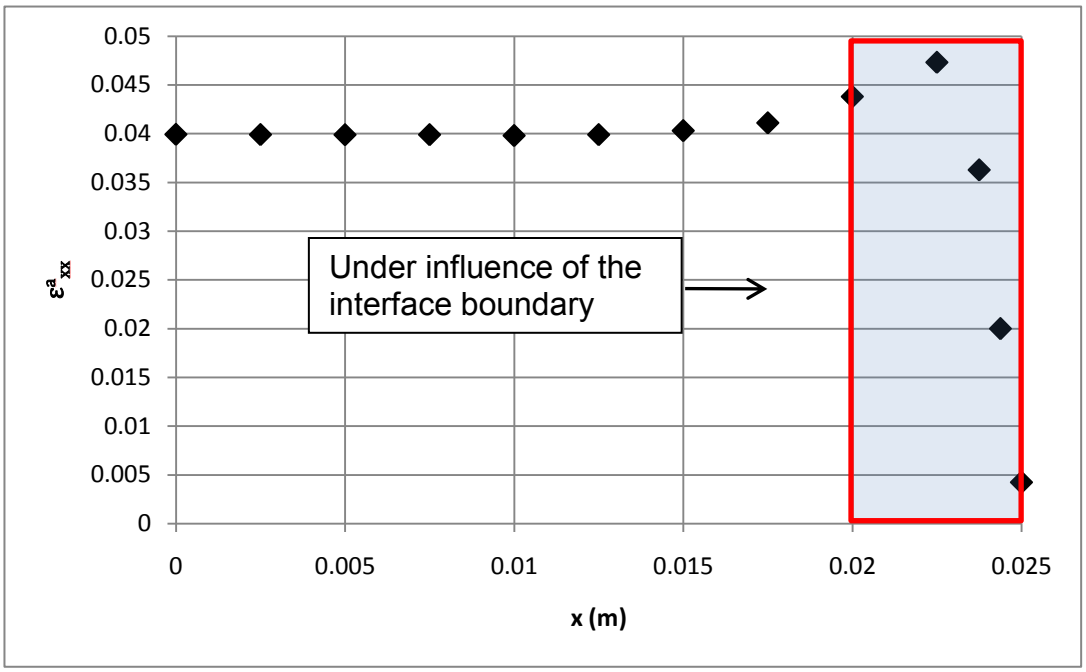

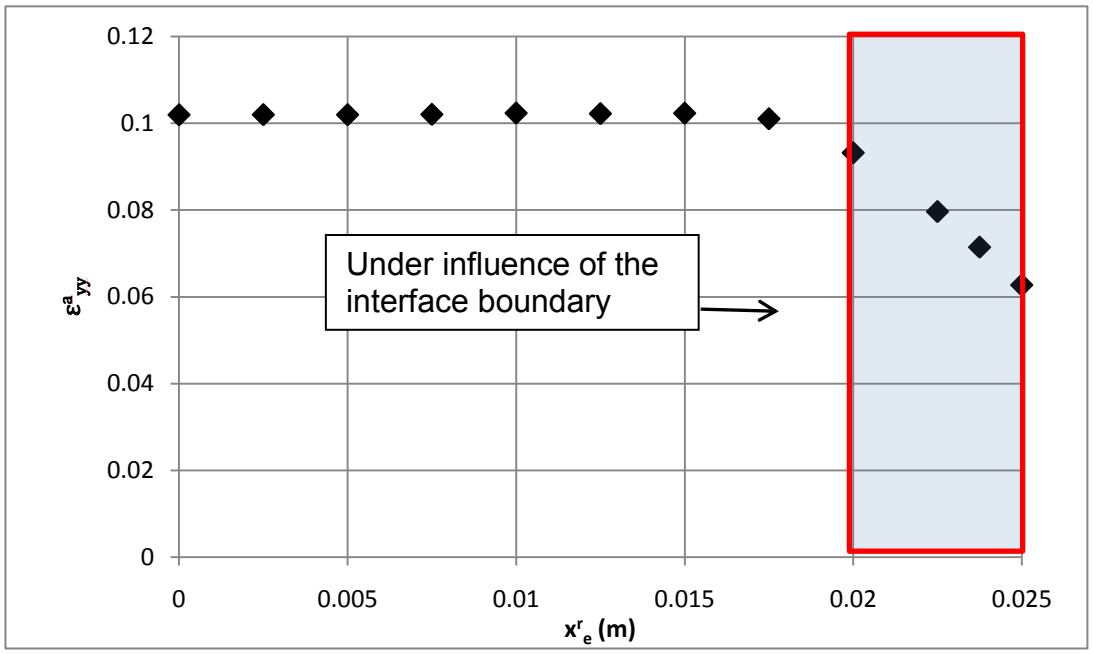

Fig. 4-3 The selected points along the DEA length have a uniform strain distribution. However, the points highlighted in red are under influence of the interface boundary between the two bodies and were neglected in our calculations.

4.2 Numerical Results

The electromechanical performance of the DEA is investigated under different loading conditions. The comparison of the numerical results from the FEA with those provided by closed-form solutions demonstrates the consistency of the models.

4.2.1 Deformation Analysis

Figures (4-4) and (4-5) depict the in-plane strain-electric field curves, and the corresponding displacement-electric field curves for four different stretch conditions. As results demonstrate, increasing n significantly increases the strains in both directions. In addition, the more the materials are pulled in one direction, the thinner they become in other directions. Thus, the electrostatic pressure acting along the thickness of the film considerably increases for a fixed amount of applied voltage, and enhances the deformation. The comparison of the planar strains for each condition shows the strain in the prestrain direction ε_{xx}^{a} is always smaller than the strain in the other direction ε_{yy}^{a}. Nonetheless, this is proven by simplifying the equations (3-24) and (3-25). Thus:

$$\frac{\varepsilon_{yy}^{a}}{\varepsilon_{xx}^{a}} = \frac{x_s^p}{(\nu+1)x_e^p + x_s^p} > 1 \Rightarrow \varepsilon_{yy}^{a} > \varepsilon_{xx}^{a} \qquad (4\text{-}4)$$

As demonstrated, active strains of approximately 0.042 and 0.1, and active displacements of approximately $2.5mm$ and $3.5mm$ were computed respectively along $x-$ and $y-$ directions for prestrain condition $n=2$.

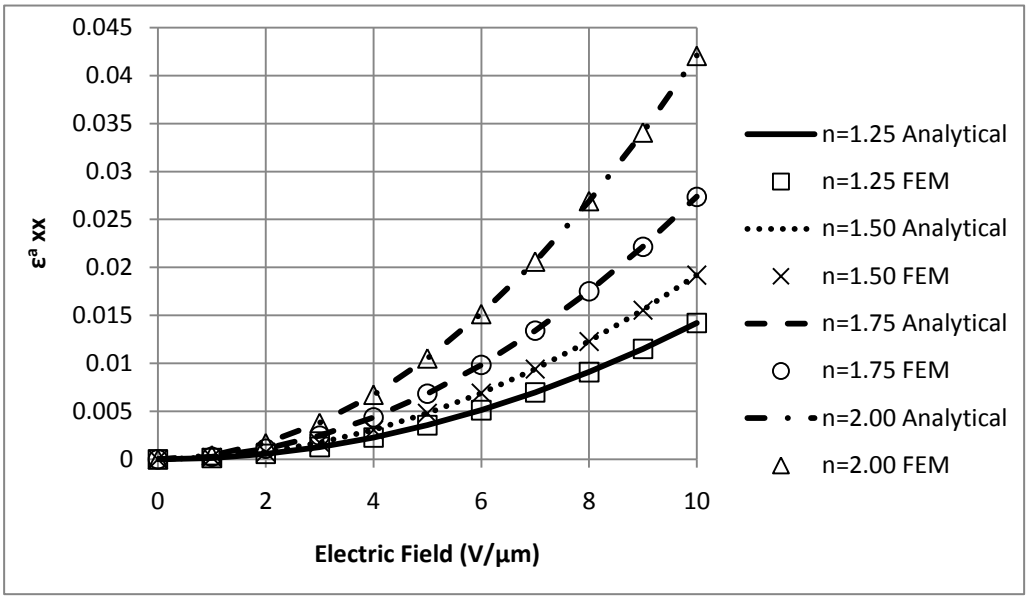

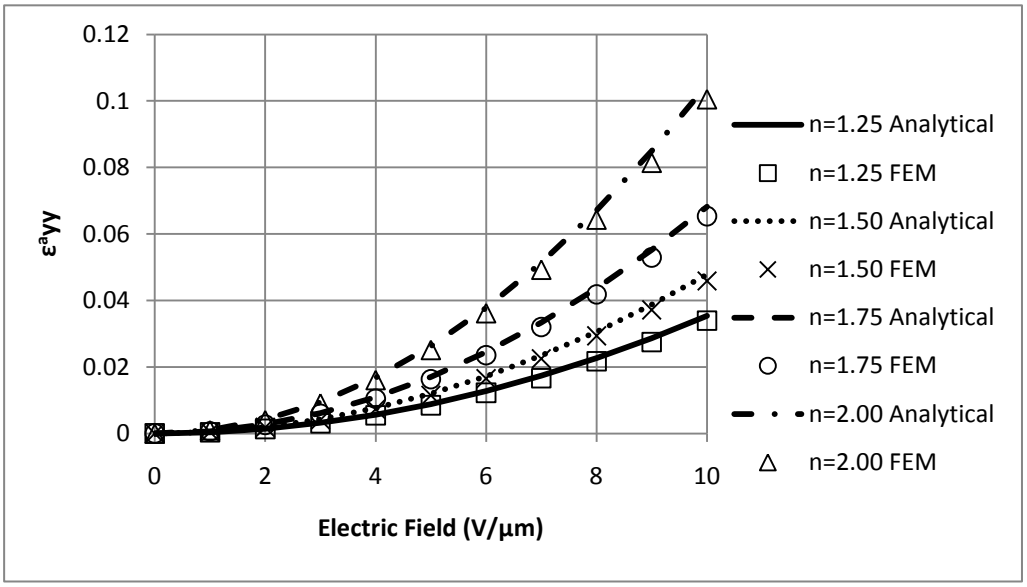

Fig. 4-4 Comparison of the numerical results of the in-plane active strains, computed by the analytical and FEM based models for different prestretch ratios.

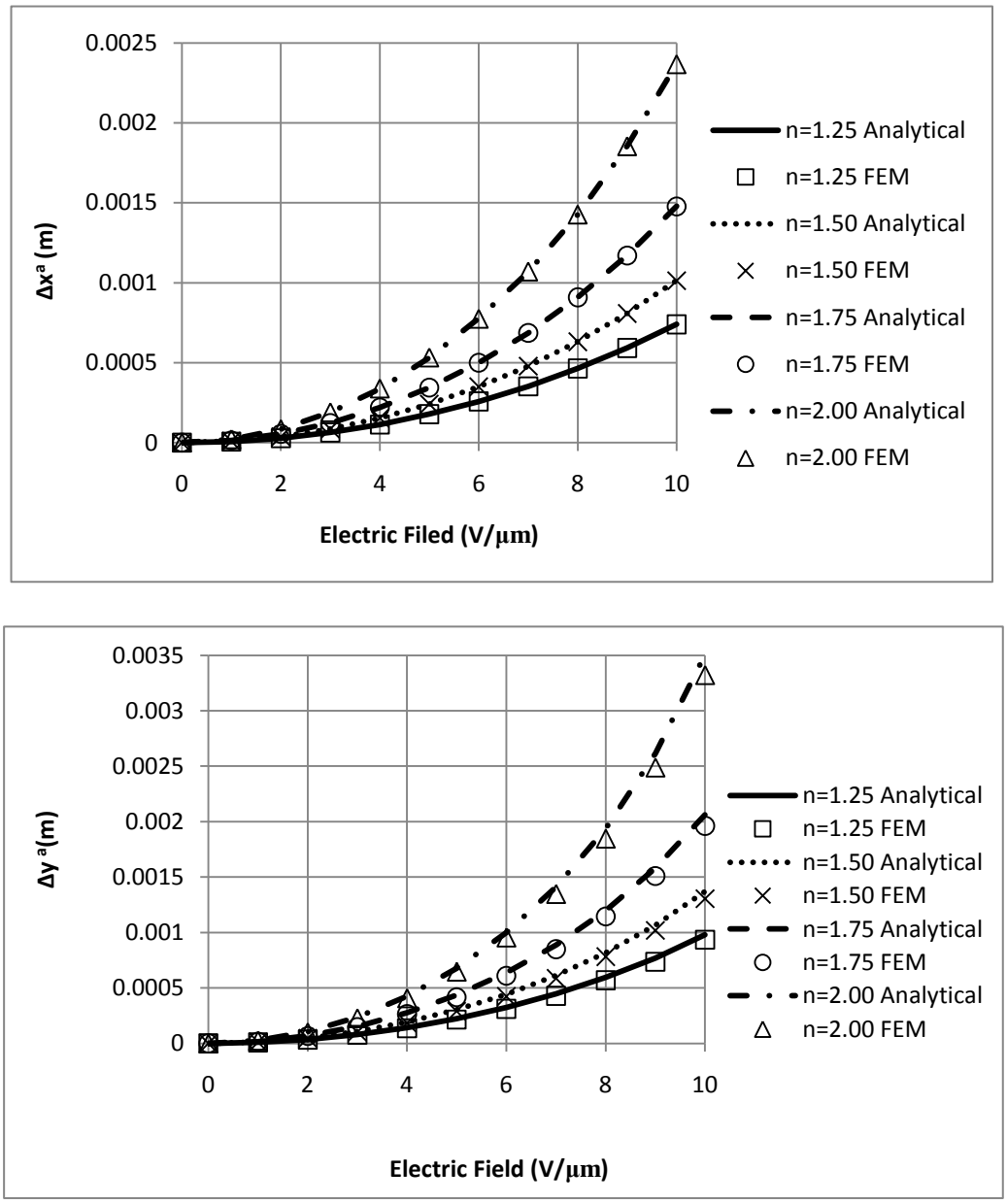

Fig. 4-5 Comparison of the numerical results of the in-plane active displacements, computed by the analytical and FEM based models for different prestretch ratios.

4.2.2 Electrode Length-to-Total Length Variation

The active stress σ_{xx}^{a} acting on the DEA, eq. (3-17), depends on the electrostatic pressure P, and the ratio of electrode length-to-total DE length. Considering a constant total length of the quarter-model at prestrain, we can rewrite the equation as:

$$\sigma_{xx}^{a} = -\nu P \chi \tag{4-5}$$

where, χ is defined as the ratio $\left(x_e^p / (x_s^p + x_e^p)\right)$. As computed in eq. (3-19) and (3.20) the active strains ε_{xx}^{a} and ε_{yy}^{a} are linearly proportional to σ_{xx}^{a}. Subsequently, they change in response to different values of χ. The schematic model of DEA configuration for different χ ratios is illustrated in fig. (4-6).

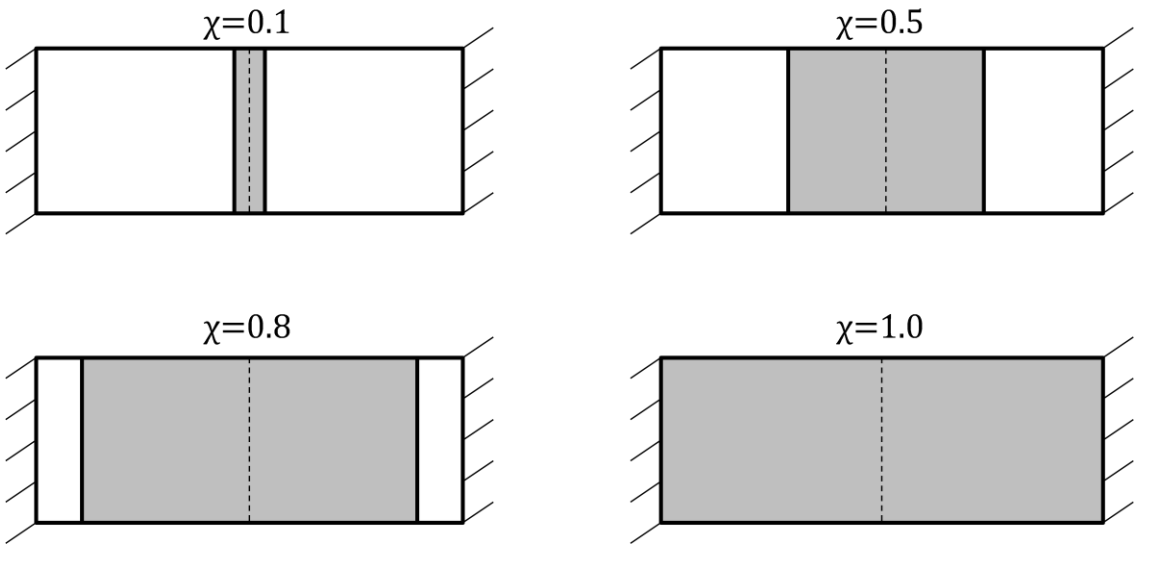

Fig. 4-6 The schematic of the DEA with different χ ratios. The dark gray and the light gray segments respectively correspond to the electrodes and the uncoated segments.

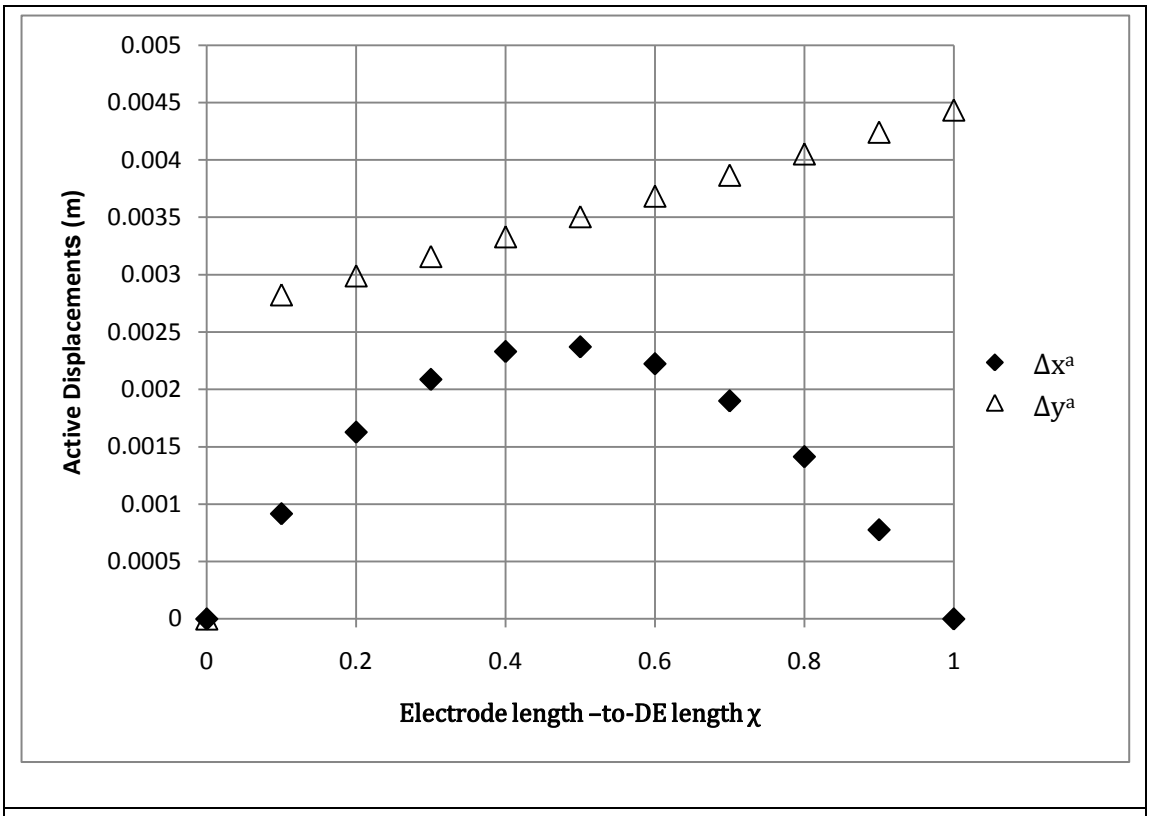

Fig. 4-7 FEM results of the active displacements obtained for each χ configuration under applied fields of up to 10 V/μm.

As assumed, the DEA is prestretched along its length ($x-$direction). Therefore, the active strain ε_{xx}^{a} is a function of the electrode length and DE length, see eq. (3-24). Thus, it can be written in terms of χ.

$$\varepsilon_{xx}^{a}=\frac{\nu\varepsilon_0\varepsilon_r\left(1-\chi\right)}{E}\left(\frac{V}{z_e^p}\right)^2 \tag{4-3}$$

As shown in eq. (3-25), the ε_{yy}^{a} do not have any direct dependencies on initial lengths and is linearly proportional to σ_{xx}^{a}, which is a function χ.

Fig. (4-7) depicts the active planar displacements for different χ. As demonstrated, for $\chi=0$ where the electrode lengths are zero the DEA deformation is zero. For $\chi=0.5$ the DEA displacement is respectively $2.5mm$

and $3.5mm$ along the $x-$ and $y-$directions. For $\chi = 1$, the DEA deformation is blocked along the $x-$direction due to the boundary condition. As a result, the DEA deformation in the $y-$direction (uniaxial) is the greatest.

5: EXPERIMENTATION

5.1 DEA Fabrication Process

In the following sections, the fabrication procedure of the DE and compliant electrodes is explained.

5.1.1 Dielectric Elastomer (DE)

The dielectric elastomer was made from a three-component silicone, commercially available as $TC-5005A/B-C$. The A/B components are a room temperature vulcanizing rubber intended primarily for making silicone skins, but is also used as a general purpose, high strength rubber. It is processed by adding the curing agent B at a ratio of 10 parts by weight to 100 parts by weight of A. In addition, the component C is added up to 45% to the total weight of A/B. This increases the flexibility and reduces the amount of force required to elongate the materials.

For best results, the materials were mixed in ultra-sonic bath for $8-10$ minutes. Thereafter, the low viscosity mixture was poured into a mould, and refrigerated few hours. This helps to release the air molecules trapped in the mixture. Afterwards, the mould was placed on a leveled shelf, and left to cure. The curing time of process was between $16-24$ hours. As we discuss further, it is important to obtain DE layers with uniform thickness. For this reason, the shelf was leveled each time prior to fabrication through four strings attached from the

ceiling to its four sides. The moulds were made from plexiglas. Plexiglas has low surface energy, which allows the materials to be demoulded easily once cured.

5.1.2 Conducting Electrodes

The electrodes were made from the mixture of polymer-carbon black [13, 40]. The mixture was processed by adding trichloroethylene at a ratio of $20mL$ to $1gr$ of a single component silicone rubber, commercially available as $CAF4-Rhodorsil$. The materials were mixed in a clean container, until the silicone completely dissolved in the solvent. Afterwards, $0.8gr$ of carbon black known as $Vulcan-XC72R$ was added up to the mixture. When the mixture was left to itself, the carbon black sank to the bottom and took up the lower 5% of the container. To make sure the carbon black particles were evenly distributed, the mixture is subjected to ultra-sonic bath for $8-10$ minutes. Left to itself, the carbon black suspension collapsed very little, and the mixture was homogenous.

Thereafter, the mixture was smeared on the DE using a thin brush with soft hairs. It took less than an hour for trichloroethylene to evaporate in open air, and leave the surface of the polymer. Once the electrodes were dried, they were nearly as compliant as the DE materials. Thus, they showed a relatively good mechanical performance.

5.2 Supply

The voltage was applied to the electrodes using a miniaturized DC-to-HV DC amplifier $(EMCO-Q101N5)$. The input voltage of the HV, $0-5V$, was delivered by a DC voltage supply $(GPC-1850D)$. The output voltage, $0-10kV$,

was connected to electrodes via thin strips of copper tape. Generally, HV amplifiers are able to absorb and dissipate the DEA energy once discharged [8]. Therefore, they allow the controlling of DEA's charging and discharging. The voltage supply only permits HVs with an increasing activation voltage level. When the voltage level was reduced the DEA reached the lower activation by gradually self discharging. For a complete deactivation and a rapid discharge of the DEA, an additional short circuit switch was used.

5.3 Physical Measurements of DEA Deformation

Two DEA were fabricated with $\chi = 0.5$ and $\chi = 1$ configurations, see fig. (5-1). Based on our calculations, the DEAs with these configurations were predicted to have the maximum active displacements respectively along $x-$ and $y-$ directions, see fig. (4-7). The DE layers were $100 \times 25 mm^2$ with a thickness of $1mm$. In $\chi = 0.5$ configuration, the $50 \times 23 mm^2$ electrodes were painted in the center of the DE on top and bottom, fig. (5-1a). In $\chi = 1$ configuration, the $98 \times 23 mm^2$ electrodes were covered the whole DE layer on top and bottom, fig. (5-1b).

Once the DEA is electrically charged, the electric field does not end abruptly at the edges of the electrodes and deviates from one electrode to another. Thus, to prevent this effect, the DE was kept uncoated approximately $1mm$ from edges in both configurations. These edges were not included in the adapted models. Both specimens were prestretched twice by their initial length, and clamped on both sides.

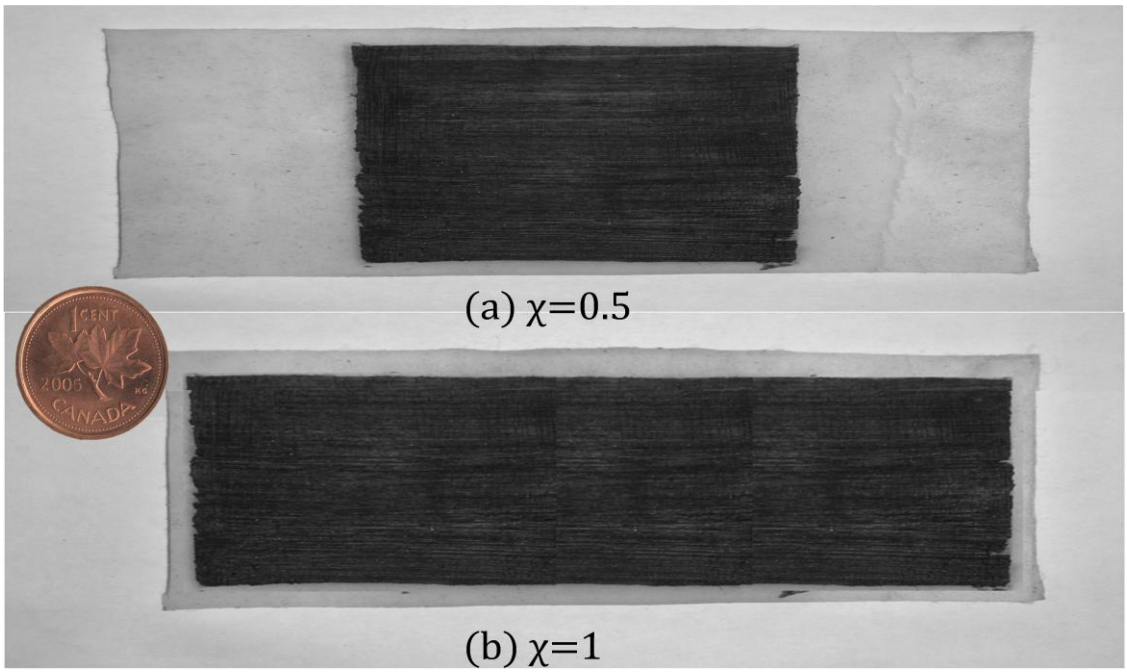

Fig. 5-1 Fabricated DEA samples (a) χ=0.5 configuration where the electrodes have the same length of the uncoated DE (b) χ=1 configuration where the electrodes have continuously covered the DE surface.

Measurements were obtained by post-processing (Vision Builder Software, National Instrument) images taken with a high-resolution camera during the expansion. As depicted in fig. (5-2), the physical results of the DEA deformation have similar trends with those numerically computed by the analytical and FEM models. Both models are based on the linear elasticity hypothesis for the DE film. They can predict the overall performance of the fabricated DEAs, which are hyperelastic in reality.

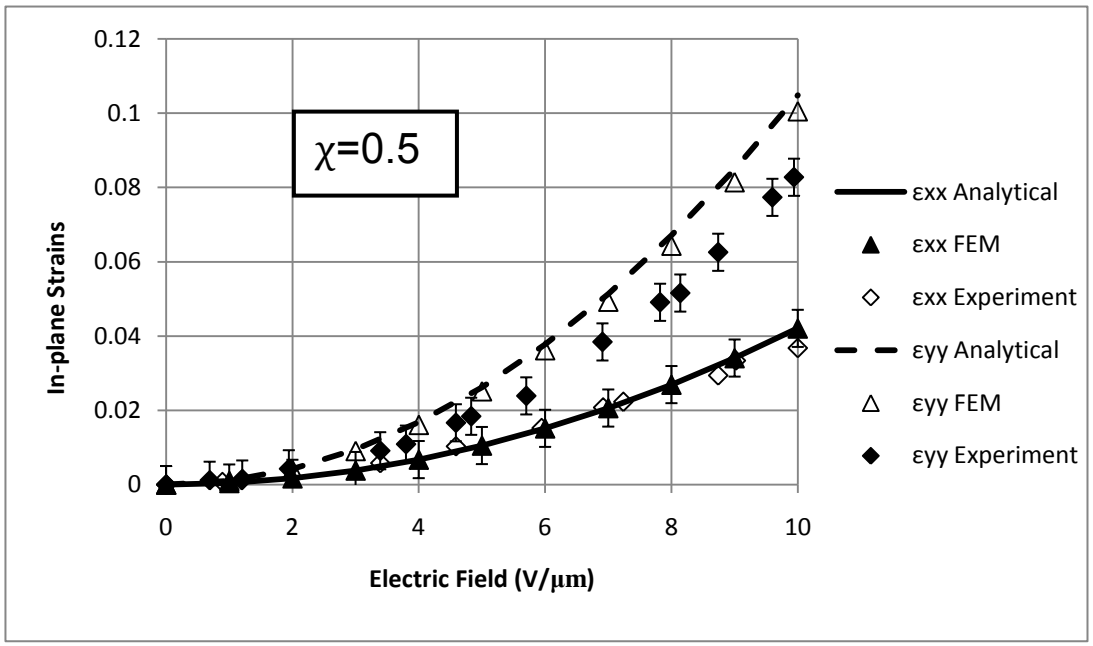

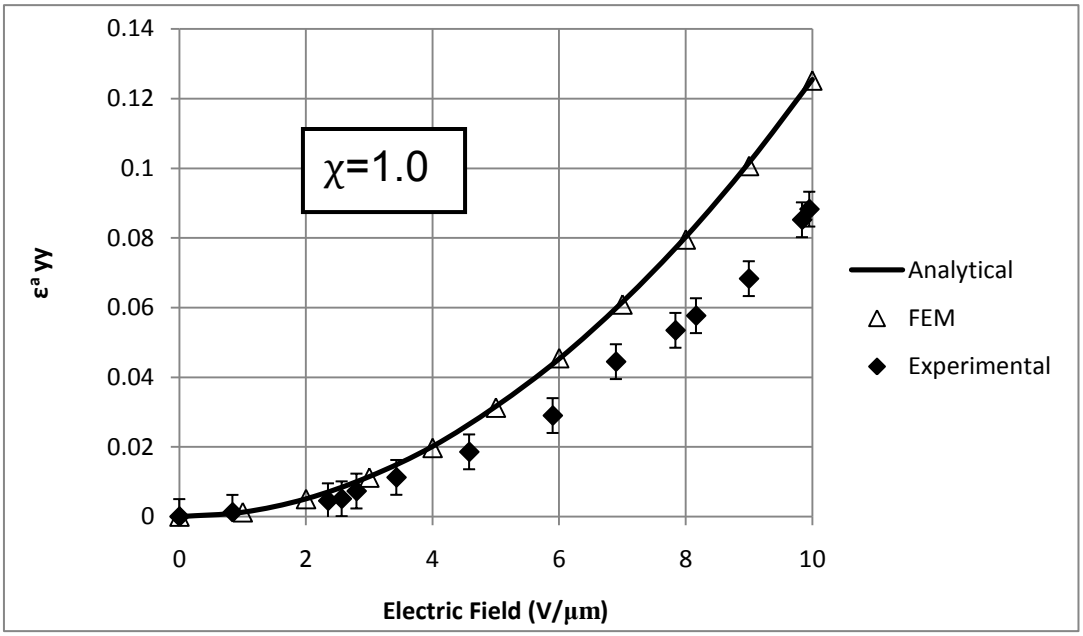

Fig. 5-2 Comparison of the physical measurements of the in-plane active strains with those computed by analytical and FEM-based models, of the DEA with χ=0.5 configuration.

5.4 Practical Issues of DEA

Experiments with DEAs made of $TC-5005A/B-C$ for DE and $Vulcan-XC72R$ for electrodes, showed that dielectric breakdown does not regularly occur instantly after activation; instead it is delayed by several seconds. The thickness of the expanding DE film continuously decreases and the electric field across the dielectric gradually increases until the dielectric strength of the film is exceeded. Dielectric break down was associated with the electrically discharge of DEA, voltage drop, and instantaneous contraction of DEA [8, 13]. The thermal dissipation of the stored electrical energy released during the breakdown, permanently damages the DEAs. We did not have appropriate instruments to measure the leakage current and occurrence time of breakdown. According to $EMCO$ data sheet, the maximum output current of the HV amplifier is $50\mu A$.

Imperfections in the DEA may also induce dielectric breakdowns [13]. This is when the electric field is increased locally and/or the DE has locally reduced the dielectric strength. For instance, geometrical flaws in the DE layer during the fabrication process, such as non-uniform thickness, may cause non-uniform electric field distribution, which provokes a non-uniform equivalent electrostatic pressure distribution across the film [8]. As a consequence, the DE deformation is more in the regions where stronger electric fields appear.

Some other reasons for non-uniform deformation of the DEA might have been due to the nonhomogeneous stiffness of the DE and compliant electrodes,

wrinkling of the film in proximity of constrained regions, and nonhomogeneous distribution of free charges on electrodes [8, 13].

5.5 HS Fabrication

The hinge has a structural frame made of carbon fiber reinforced plastic (CFRP), and three compliant joints, which were obtained by embedding a $125\mu m$ polyamide film commercially available as Kapton, in-between two sheets of CFRP. The composite structure is very lightweight, and has a high stiffness-to-weight ratio. The polymer joints act as revolute joints each having one rotational DOF with the ability to bend repeatedly without tearing apart, or losing its flexure. Fig. (5-3) illustrates the HS with three revolute joints and four links.

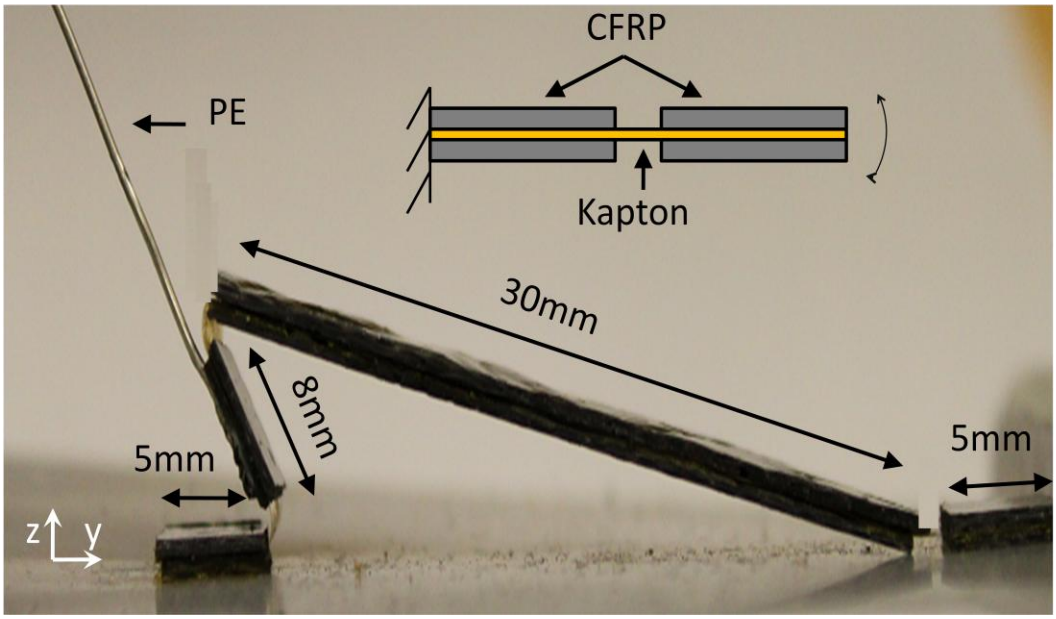

Fig. 5-3 The HS mounted on the DE surface is comprised of 3 flexible joints and 4 links.

As computed in eq. (3-33), the angular displacement of the HS, α, depends on the DEA active displacement DEA along the y-direction, Δy^a. Therefore, to achieve the largest angle change the DEA with $\chi = 1$ (maximum uniaxial active strain) configuration was used. Fig. (5-4) depicts the variation of α and Δy^a under the applied electric fields. As demonstrated in fig (5-4), the actuator was able to rotate the PEs by 35°.The initial angle of the structures before the activation were measured to be 30°.

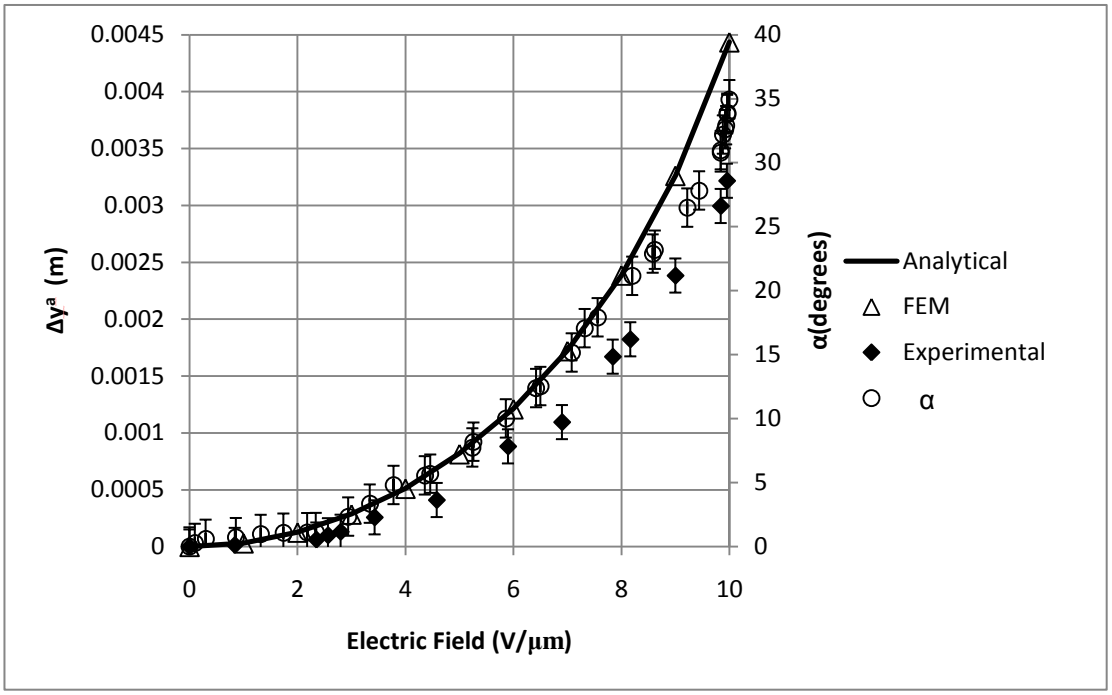

Fig. 5-4 The physical measurements of the active uniaxial displacement of the DEA and the angular displacement of the HS under applied fields.

5.6 Antenna System

The MCA (discussed in section 2.1) has been implemented; see fig. (5-5). The monopole is tuned at $0.95GHz$ and located at the centre of a square

$(450 \times 450 mm^2)$ copper GP. A pair of V-shaped PEs is located symmetrically at the two sides of the monopole at a distance of a tenth-wavelength. The PEs are made of aluminium, and are a half-wavelength long. The angle between the PE arms, γ, is a 60° constant. The PE counter-rotation is to reduce the impedance variations of the monopole. Slant angle of the PEs, β, is defined as an angle between the closer PE arm to the GP and the GP. The slant angle is computed by subtracting 30° from α.

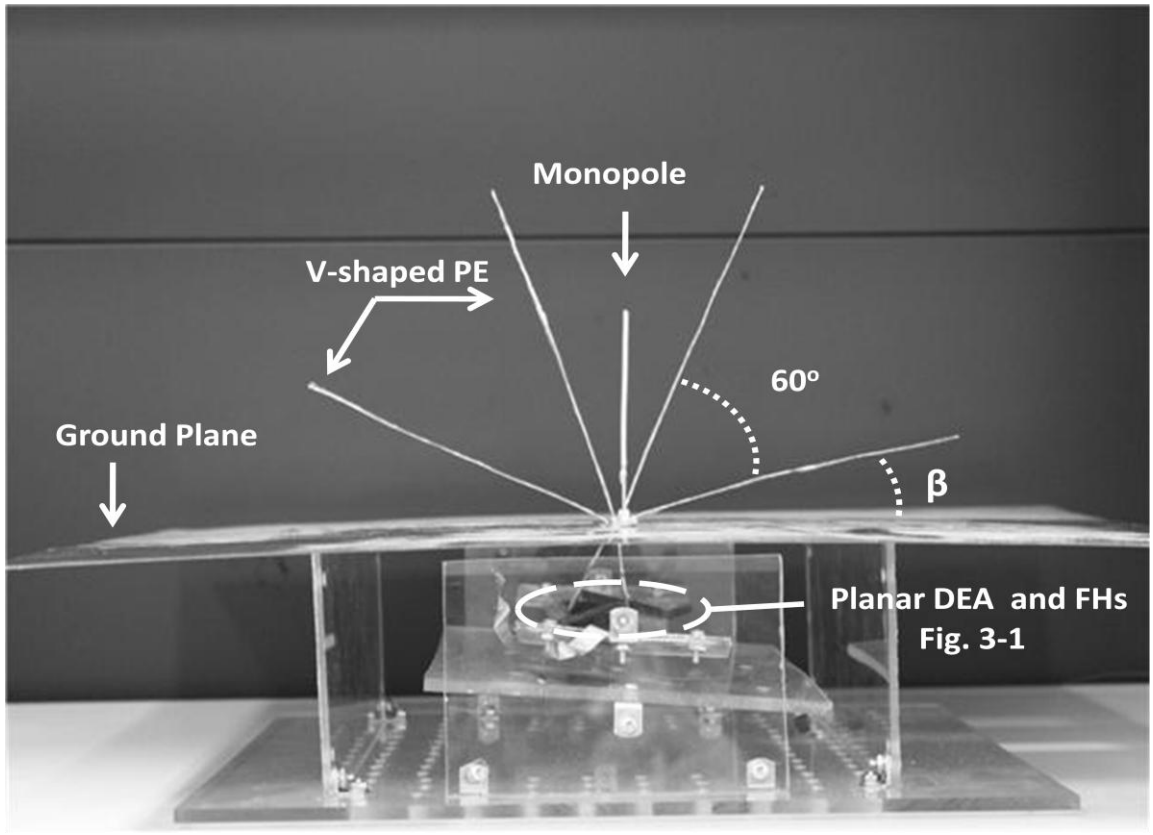

Fig. 5-5 The implemented tuneable antenna prototype based on the PE counter rotation, actuated by means of the DEA. The actuation mechanism is located beneath the GP electrically isolated from the antenna system.

The physical measurements of the RP were obtained from the anechoic chamber. Fig. (5-6) depicts the physical setup of the antenna.

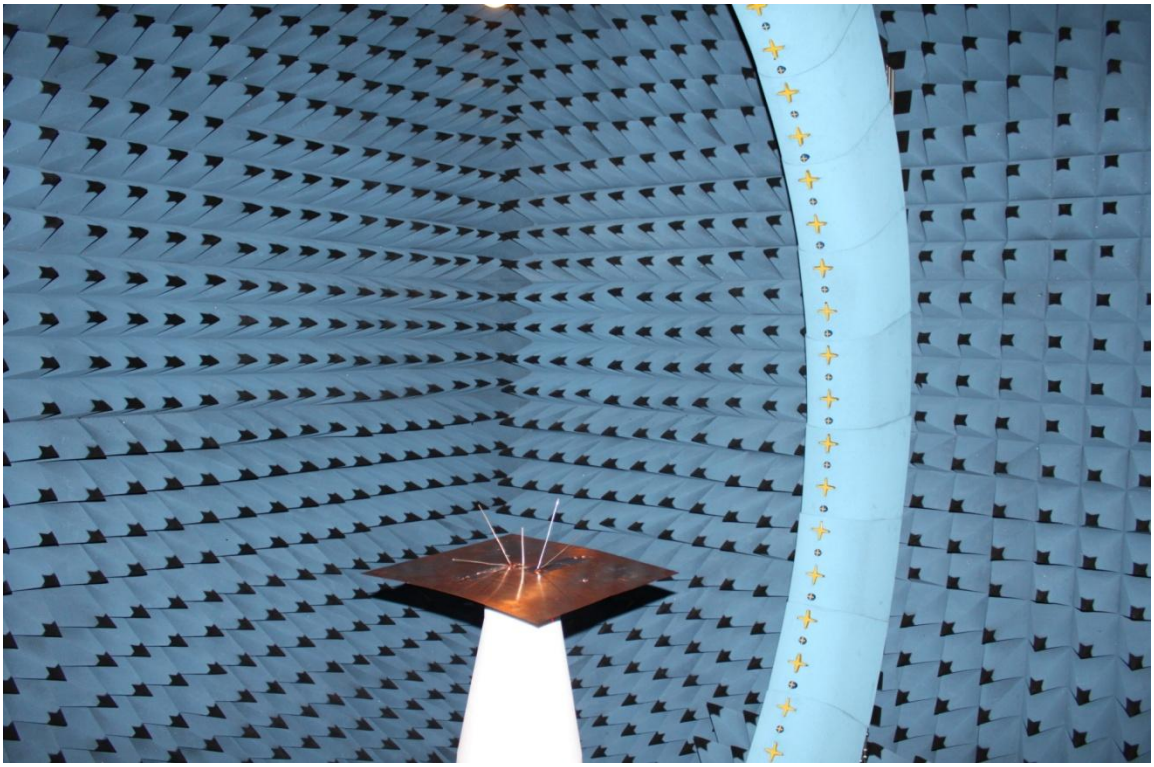

Fig. 5-6 Depicts the antenna setup. The RP measurements were obtained from the anechoic chamber.

For sake brevity, only the most significant pattern variations at $0.95GHz$ are presented in the $E-$plane, although pattern variations were also observed in $H-$plane. Fig. (5-7) depicts the patterns in $E-$plane for different values of spherical coordinate θ, see the coordinate system in fig. (5-7). As demonstrated, variations of β due to the angular displacement of the parasitic elements lead to variations of the far-field radiation pattern of the monopole. Therefore, decorrelated patterns are available. This is while the impedance variation was

fairly preserved. Fig. (5-8) demonstrates the physical measurements of the reflection coefficient S_{11}.

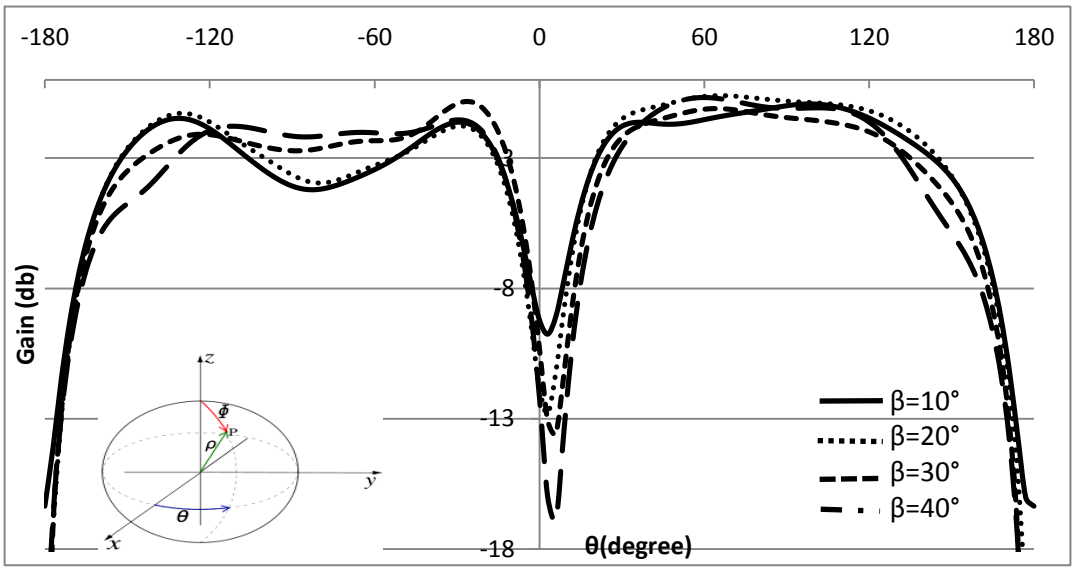

Fig. 5-7 Physical measurements of the RP variations for four different PE slant angles

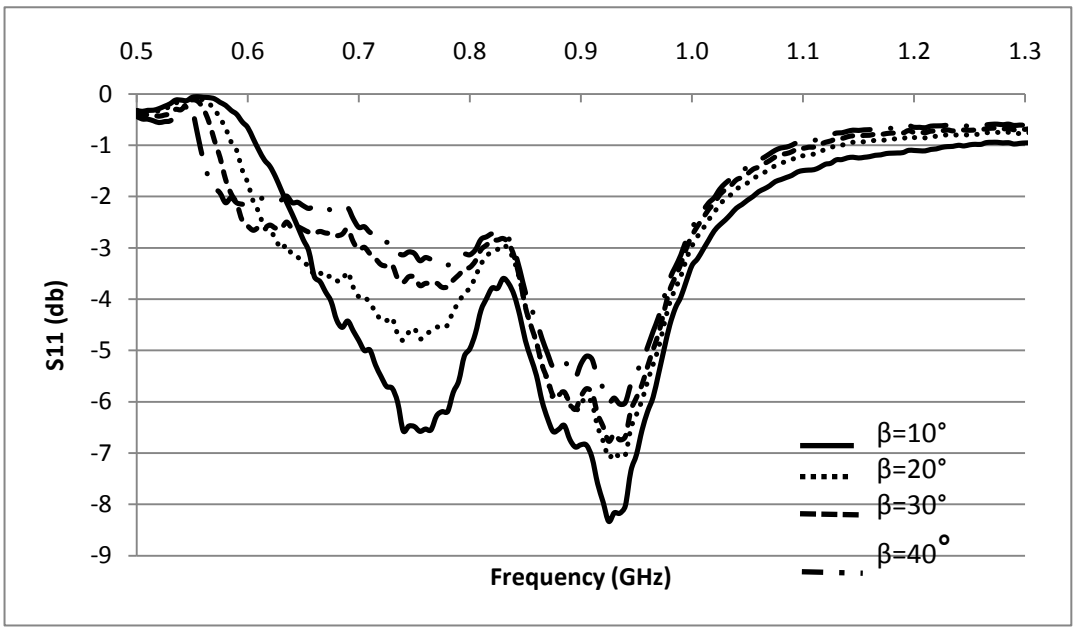

Fig. 5-8 Physical measurements of the reflection coefficient at the monopole for four different slant angles

6: CONCLUSION

The developed planar dielectric elastomer showed to be suitable for implementing the proposed pattern reconfigurable antenna. Specifically, the elastomer was able to rotate the pair of V-shaped parasitic elements within the range required to record significant pattern variations of the antenna.

The developed mechanical analytical model, although simplified, showed to correctly predict the planar deformations of the fabricated dielectric elastomer. In fact, deformations recorded during mechanical tests were consistent with the predictions of the model. The analytical model was used to optimize the length of the dielectric elastomer electrodes. Specifically, the elastomer with $\chi = 0.5$ and $\chi = 1$ had maximum active displacements respectively along the longitudinal ($x-$ axis) and transversal ($y-$axis) directions of the actuator.

The transversal deformation of the fabricated dielectric elastomer with $\chi = 1$ was measured to be approximately $4.5mm$ when electrically activated with $10V/\mu m$. Each carbon fiber-reinforced plastic hinge converted this maximum deformation of the elastomer to 35° rotation of each V-shaped parasitic element. The counter-rotation action of the two PEs, achieved by fixing them to two asymmetrically oriented hinges, reduced the impedance variation of the antenna. The performed preliminary experimental tests showed that the variation of the

radiation pattern of the antenna, caused by the rotation of the PEs, was noticeable.

APPENDICES

Appendix A: Hooke's Law of Elasticity [10]

The generalized Hooke's Law is used to predict the deformations caused in a given material by an arbitrary combination of stresses. In equilibrium, the stress is decomposed in to three mutually orthogonal components. One component acts perpendicular to the surface and represents the normal stress, and the other two components acting tangential to the surface, which represent the shear stresses. It is possible to describe the strain conditions at a point with the deformation components (u,v,w) in 3D and their derivatives. Following the small deformation assumption the components of the normal strain and the components of the shear strains are given in equations (A-1)-(A-6)

$$\varepsilon_{xx}=\frac{\partial u}{\partial x} \qquad \varepsilon_{yy}=\frac{\partial v}{\partial y} \qquad \varepsilon_{zz}=\frac{\partial w}{\partial z} \qquad \text{(A-1)- (A-3)}$$

$$\varepsilon_{xy}=\frac{1}{2}(\frac{\partial u}{\partial x}+\frac{\partial v}{\partial y}) \qquad \varepsilon_{yz}=\frac{1}{2}(\frac{\partial v}{\partial y}+\frac{\partial w}{\partial z}) \qquad \varepsilon_{xz}=\frac{1}{2}(\frac{\partial u}{\partial x}+\frac{\partial w}{\partial z}) \quad \text{(A-4)- (A.6)}$$

The symmetric strain tensor ε containing both normal strains and shear strains components:

$$\varepsilon=\begin{bmatrix}\varepsilon_{xx} & \varepsilon_{xy} & \varepsilon_{xz}\\ \varepsilon_{xy} & \varepsilon_{yy} & \varepsilon_{yz}\\ \varepsilon_{xz} & \varepsilon_{yz} & \varepsilon_{zz}\end{bmatrix} \qquad \text{(A.7)}$$

The stress in a material is described by the symmetric stress tensor σ, eq. (A-8), consists of three components of normal stress $(\sigma_{xx}, \sigma_{yy}, \sigma_{zz})$ and six, or if symmetry used three components of shear stress

$$\sigma = \begin{bmatrix} \sigma_{xx} & \sigma_{xy} & \sigma_{xz} \\ \sigma_{yx} & \sigma_{yy} & \sigma_{yz} \\ \sigma_{zx} & \sigma_{zy} & \sigma_{zz} \end{bmatrix} \quad \text{(A-8)}$$

where,

$$\sigma_{xy} = \sigma_{yx}, \sigma_{xz} = \sigma_{zx}, \sigma_{yz} = \sigma_{zy} \quad \text{(A-9)}$$

The stress-strain relationship for linear condition is:

$$\sigma = D.\varepsilon \quad \text{(A-10)}$$

where, D is the elasticity matrix and the stress-strain components are described in vector form where the six components of stress and stress in column vectors defined as:

$$\varepsilon = \begin{bmatrix} \varepsilon_{xx} \\ \varepsilon_{yy} \\ \varepsilon_{zz} \\ \varepsilon_{xy} \\ \varepsilon_{yz} \\ \varepsilon_{zx} \end{bmatrix} \qquad \sigma = \begin{bmatrix} \sigma_{xx} \\ \sigma_{yy} \\ \sigma_{zz} \\ \sigma_{xy} \\ \sigma_{yz} \\ \sigma_{zx} \end{bmatrix} \quad \text{(A-11)- (A-12)}$$

The elasticity matrix D and the more basic matrix D^{-1} (the inverse of D, also known as the flexibility or compliance matrix are defined for isotropic, orthotropic, and anisotropic materials). For isotropic material, the D^{-1} looks like

$$D^{-1} = \frac{1}{E}\begin{bmatrix} 1 & -\nu & -\nu & 0 & 0 & 0 \\ -\nu & 1 & -\nu & 0 & 0 & 0 \\ -\nu & -\nu & 1 & 0 & 0 & 0 \\ 0 & 0 & 0 & 1+\nu & 0 & 0 \\ 0 & 0 & 0 & 0 & 1+\nu & 0 \\ 0 & 0 & 0 & 0 & 0 & 1+\nu \end{bmatrix} \tag{A-13}$$

Inverting D^{-1} symbolically results in the following definition of D:

$$D = \frac{E}{(1+\nu)(1-2\nu)}\begin{bmatrix} 1-\nu & \nu & \nu & 0 & 0 & 0 \\ \nu & 1-\nu & \nu & 0 & 0 & 0 \\ \nu & \nu & 1-\nu & 0 & 0 & 0 \\ 0 & 0 & 0 & 1-2\nu & 0 & 0 \\ 0 & 0 & 0 & 0 & 1-2\nu & 0 \\ 0 & 0 & 0 & 0 & 0 & 1-2\nu \end{bmatrix} \tag{A-14}$$

Appendix B: Derivation of the Maxwell's Pressure [14]

In principle, dielectric EAP is a flexible capacitor, constructed with an elastic polymer for dielectric and compliant conductive coatings for electrodes. When the capacitor is electrically charged with DC voltage (kilovolts), the contraction between the opposing charges on the electrodes compress the elastic dielectric in the direction of the generated electric field. Thus, the nearly incompressible dielectric film expands in plane directions.

The electrostatic pressure acting on the elastic dielectric can be calculated for any given applied voltage and dielectric thickness. The repelling forces between equal charges on the two electrodes help the planar expansion as well. Given the elasticity of the elastic dielectric film, the flexible capacitor returns to its initial state when the voltage is switched off and the capacitor is discharged. This electromechanical coupling transforms electrical energy directly to mechanical work, and produces large strains.

We start from the eq. (B-1), the capacitance C of the capacitor, in order to derive the solution for the electrostatic perssure,

$$C = \varepsilon_0 . \varepsilon_r \frac{A}{z} \qquad \text{(B-1)}$$

Where, ε_0 is the vaccuum permitivitty equal to $8.85 \times 10^{-12} F/m$, ε_r is the relative dielectric constant with negligible variations, A is the area, and z is the thickness of the dielectric elastomer.

The electrostatic energy U stored in the capacitor is:

$$U = \frac{1}{2}\frac{Q^2}{C} \tag{B-2}$$

where, Q and $-Q$ are the fixed charges are placed on the surface of the electrodes. Therefore, the stored energy of the capacitor is:

$$U = \frac{1}{2}\frac{Q^2.z}{\varepsilon_o.\varepsilon_r.A} \tag{B-3}$$

The electrostatic pressure P is:

$$P = \frac{1}{A}\frac{\partial U}{\partial z} \tag{B-4}$$

For a perfect elastic material, the change in the electrostatic pressure is equal to the mechanical work performed by the actuator. Once the materials are squeezed by the applied P, their shape and/or size deforms while keeping their volume constant. The mechanical constraint for a constant volume is given in the eq. (B-5):

$$\partial(volume) = \partial(A.z) = 0 \Rightarrow \partial A.z + \partial z.A = 0 \tag{B-5}$$

The change of the stored energy ∂U for a change in a thickness ∂z and an area ∂A is computed by the eq. (B-6).

$$\partial U = (\frac{1}{2}\frac{Q^2}{\varepsilon_0\varepsilon_r A})\partial z - (\frac{1}{2}\frac{Q^2 z}{\varepsilon_0\varepsilon_r})\frac{\partial A}{A} \tag{B-6}$$

From the eq. (B-5), the relation between ∂A and ∂z is defined as:

$$\frac{\partial A}{A} = -\frac{\partial z}{z} \tag{B-7}$$

By inserting the eq. (B-6) in to eq. (B-5), we can rewrite the change in the stored energy as a function of the change in the dielectric thickness as:

$$\partial U = (\frac{Q^2}{\varepsilon_0 \varepsilon_r A})\partial z \tag{B-8}$$

Thereby, the electrostatic pressure P given in the eq. (B-4) can be written as:

$$P = \frac{Q^2}{\varepsilon_0 \varepsilon_r A^2} \tag{B-9}$$

The electric field E_f is defined as:: in terms of the applied voltage V, and the dielectric thickness z:

$$E = \frac{1}{\varepsilon_0 \varepsilon_r}\frac{Q}{A} = \frac{V}{z} \tag{B-10}$$

Finally, by combining equations (B-9) and (B-10) we can write P as a function of V and z:

$$P = \varepsilon_0 \varepsilon_r (\frac{V}{z})^2 \tag{B-11}$$

REFERENCE LIST

1. Vaughan R. G., and Andersen J. B., *Antenna Diversity in Mobile Communications,* IEEE Trans. Vehicular Technology, 1987, 36(4): p. 149-172
2. Mahanfar A., Menon C., and Vaughan R.G., *Electroactive Polymers for Deformable Parasitic Elements,* Electronics Letters, 2008, 44(19)
3. Washington G., *Design, Modeling, and Optimization of Mechanically Reconfigurable Aperture Antennas,* IEEE Trans. Antennas and Propagation, 2002, p. 628-637
4. Vaughan R.G., *Switched Parasitic Elements for Antenna Diversity,* IEEE Trans. Antennas and Propagation, 1999, 47(2): p. 399-405
5. Mahanfar A., Menon C., Vaughan R. G., *Tuneable Dielectric Resonator Antennas Using Voltage-Controlled Mechanical Deformation.* Advances in Science and Technology, Integrated Systems, 2008, p. 614-619
6. Han X., and Vaughan R. G., *Configurable Antenna Using Moving Wire Parasitic Elements,* IEEE Trans. Antennas and Propagation, 2010, p. 44-47
7. Roy D. K., Perline R., Pei Q., *Electroelastomers: Applications of Dielectric Elastomer Transducers for Actuation, SPIE, Smart Structures*. 2002, 4698: p. 254-270
8. Lochmatter P., *Development of a Shell-like Electroactive Polymer (EAP) Actuator*, PhD. Thesis, Mechanical and Process Engineering, Swiss Federal Institute of Technology Zurich. 2007, p. 340
9. Perline R., Pei Q., Kombluh R. D., *Dielectric Elastomer Artificial Muscle Actuators Toward Biomimetic Motion*, SPIE, 2002, 4695: p. 126-137
10. Ward I.M., and Sweeney J., *An Introduction to the Mechanical Properties of Solid Polymers,* 2nd Edition, John Wiley & Sons Inc., 2004, p. 394-400
11. Bar-Cohen Y., *Electroactive Polymers as an Enabling Materials Technology,* Proceedings of the Institution of Mechanical Engineers, Part G, Aerospace Engineering, 221(4): p. 553-564
12. Dai L., *Stimuli-responsive Polymers*, Intelligent Macromolecules for Smart Devices, Springer, London, 2004, p. 81
13. Kofod G., *Dielectric Elastomer Actuators*, PhD. Thesis, Department of Chemistry, Technical University of Denmark: Copenhagen, 2001, p. 139
14. Pelrine R., Kornbluh R. D., and Joseph J.P., *Electrostriction of Polymer Dielectrics with Compliant Electrodes as a Means of Actuation,* Tenth IEEE International Workshop, Micro Electro Mechanical Systems, 1998, 64(1): p. 77
15. Wissler M., and Mazza M., *Electromechanical Coupling in Dielectric Elastomer Actuators,* Science Direct, Sensors and Actuators, 2007, 138(2): p. 384

16. Biddiss E., and Chau T., *Electroactive Polymeric Sensors in Hand Prostheses,* Science Direct, Medical Engineering and Physics, 2006, 28(6): p. 568

17. Pelrine R., Kombluh R. D., and Pei Q., *High-field Deformation of Elastomeric Dielectrics for Actuator, Science Direct,.* 2000, 11(2): p. 89

18. Fergal O.M., *A Review on Dielectric Elastomer Actuators: technology, applications, and challenges,* Applied Physics, 2008, 104(7): p. 071101

19. Barnes A. Z., Liu A. Z., and Young Q., *Evaluation of Selected Dielectric Elastomers for Use in an Artificial Muscle Actuator*, Australian Robotics and Automation Association, 2007

20. Carpi F., Chiarelli P., Mazzoldi A., *Electromechanical Characterisation of Dielectric Elastomer Planar Actuators: Comparative Evaluation of Different Electrode Materials and Different Counter-loads,* Science Direct, Sensors Actuators, 2003, 107(1): p. 85

21. Bar-Cohen Y., *Electroactive Polymer (EAP) Actuators as Artificial Muscles. Reality, Potential, and Challenges.* SPIE, 2004, 5385, p. 10-16

22. Wissler M.T., *Modeling Dielectric Elastomer Actuators*, *Mechanical and Process Engineering*, Swiss Federal Institute of Technology, Zurich. p. 153

23. Madden J.W., *Artificial Muscle Technology: Physical Principles and Naval Prospects, IEEE Trans. Oceanic Engineering,* 2004, 29(3): p. 706

24. Carpi F., and De Rossi D., *Contractile Dielectric Elastomer Actuator with Folded Shape,* SPIE, 2006, 6168: p. 99

25. Carpi F., and De Rossi D., *A New Contractile Linear Actuator Made of Dielectric Elastomers with Folded Structure, SPIE,* 2006, 5759, p. 64-74

26. Dubois P, Rosset S., and Koster S., *Microactuators Based on Ion Implanted Dielectric Electroactive Polymer (EAP) Membranes,* Science Direct, Sensors Actuators, 2006, 130: p. 147

27. Goulbourne N, Frecker M., and Synder A. J., *Modeling of a Dielectric Elastomer Diaphragm for a Prosthetic Blood Pump,* SPIE, 2003, 5051: p. 319

28. Tews A.M., Pope K. L., and Snyder A. J., *Pressure-Volume Characteristics of Dielectric Elastomers Diaphragms*, SPIE, Smart Structures and Materials, 2003, 4854: p. 123

29. Qibing P., Kombluh R. D., and Rosenthal R., *Multifunctional Electroelastomer Roll Actuators and their Application for Biomimetic Walking Robots*, SPIE, Smart Structures and Materials, 2003, 5051: p. 281-290

30. Plante J., *Dielectric Elastomer Actuators for Binary Robotics and Mechatronics,* Massachusetts Institute of Technology, 2006

31. Soleimani M., and Carlo M., *Preliminary Investigation of a Balloon-shape Actuator Based on Electroactive Elastomers,* SPIE, Smart Materials and Structures, 2010, 19(4): p. 047001

32. Kovacs G., Lochmatter P., Wissler M., *Robotic Arm*, Science Direct, 2008, p. 279

33. Pei Q., Perline R., and Stanford S., *Electroelastomer Rolls and their Application for Biomimetic Walking robots,* Science and Technology, Synthetic Metals, 2003, 135-136: p. 129

34. Pei Q., Perline R., and Rosenthal M., *Multiple-Degrees-of-Freedom Electro-elastomer Roll Actuators,* Science Direct, 2004. 13(5): p. 86

35. Biddiss E., and Chau T., *Dielectric Elastomers as Actuators for Upper Limb Prosthetics: Challenges and Opportunities,* Science Direct, Medical Engineering and Physics, 2008, 30(4): p. 403

36. Carpi F., Menon C., De Rossi D., *Electroactive Elastomeric Actuator for All-Polymer Linear Peristaltic Pumps, I*EEE Trans. Mechatronics, 2009. 15(3): p. 460-470

37. De Rossi D., Carpi F., and Scilingo E. P., *Polymer Based Interfaces as Bioinspired Smart Skins.* Science Direct, 2005. 116(1-3): p. 165

38. Trafton A., *New Robots Mimic Fish's Swimming,* Massachusetts Institute of Technology, 2009

39. Carpi F., De Rossi D., and Gaudenzi P. D., *Martian Jumping Rover Equipped with Electroactive Polymer Actuators: A Preliminary Study.* IEEE Trans. Aerospace and Electronics Systems, 2007, (1): p. 79-99

40. Carpi F., De Rossi D., *Theoretical Description and Fabrication of a New Dielectric Elastomer Actuator Showing Linear Contractions,* Science Direct, 2004: p. 344

41. Menon C., Carpi F., De Rossi D., *Concept Design of Novel Bio-Inspired Distributed Actuators for Space Applications,* Acta Astronaut., 2009, 65(5-6): p. 825

42. Tognetti A., Quaglini R., De Rossi D., *Wearable Kinesthetic System for Capturing and Classifying Upper Limb Gesture in Post-stroke Rehabilitation,* Neuro-Engineering and Rehabilitation, 2005, 2(1): p. 8

43. Jean-Sebastian P., and Steven D., *On the Nature of Dielectric Elastomer Actuators and its Implications for their Design,* SPIE, 2006, 6168: p. 61681

44. Bar-Cohen J., Leary S. P., Shahinpoor M., *Electroactive Polymer (EAP) Actuators for Planetary Applications*, SPIE, Smart Structures and Materials, 1999, 3669: p. 57-63

45. Bar-Cohen J., *Electroactive Polymers: Current Capabilities and Challenges*, SPIE, Smart Structures and Materials, 2002, 4695: p. 1-7

46. Zhang R., *Development of Dielectric Elastomer Actuators and their Implementation in a Force Feedback Interface*, PhD Thesis, Swiss Federal Institute of Technology, Zurich, 2007, p. 200

47. Guggi K., *The Static Actuation of Dielectric Elastomer Actuators: How Does Pre-stretch Improve Actuation,* Applied Physics, 2008, 41(21): p. 215405

48. COMSOL Multiphysics Version 3.2, *Modeling Guide Handbook*, 2005

49. Carpi F., Chiarelli P., Mazzoldi A., *Electromechanical Characterisation of Dielectric Elastomer Planar Actuators: Comparative Evaluation of Different Electrode Materials and Different Counter-loads,* Science Direct, Sensors Actuators, 2003, 107(1): p. 85